JOURNAL OF GEOPHYSICAL RESEARCH, VOL. 101, NO. D1, PAGES 2087-2109, JANUARY 20, 1996

Hydrocarbon ratios during PEM-WEST A: A model perspective

S.A. McKeen,[1,2] S.C. Liu,[1] E.-Y. Hsie,[1,2] X. Lin,[1,2] J.D. Bradshaw,[3] S. Smyth,[3] G. L. Gregory,[4] and D.R. Blake[5]

Abstract. A useful application of the hydrocarbon measurements collected during the Pacific Exploratory Mission (PEM-West A) is as markers or indices of atmospheric processing. Traditionally, ratios of particular hydrocarbons have been interpreted as photochemical indices, since much of the effect due to atmospheric transport is assumed to cancel by using ratios. However, an ever increasing body of observatonial and theoretical evidence suggests that turbulent mixing associated with atmospheric transport influences certain hydrocarbon ratios significantly. In this study a three-dimensional mesoscale photochemical model is used to study the interaction of photochemistry and atmospheric mixing on select hydrocarbons. In terms of correlations and functional relationships between various alkanes the model results and PEM-West A hydrocarbon observations share many similar characteristics as well as explainable differences. When the three-dimensional model is applied to inert tracers, hydrocarbon ratios and other relationships exactly follow those expected by simple dilution with model-imposed "background air," and the three-dimensional results for reactive hydrocarbons are quite consistent with a combined influence of photochemistry and simple dilution. Analogous to these model results, relationships between various hydrocarbons collected during the PEM-West A experiment appear to be consistent with this simplified picture of photochemistry and dilution affecting individual air masses. When hydrocarbons are chosen that have negligeble contributions to clean background air, unambiguous determinations of the relative contributions to photochemistry and dilution can be estimated from the hydrocarbon samples. Both the three-dimensional model results and the observations imply an average characteristic lifetime for dilution with background air roughly equivalent to the photochemical lifetime of butane for the western Pacific lower troposphere. Moreover, the dominance of OH as the primary photochemical oxidant downwind of anthropogenic source regions can be inferred from correlations between the highly reactive alkane ratios. By incorporating back-trajectory information within the three-dimensional model analysis, a correspondence between time and a particular hydrocarbon or hydrocarbon ratio can be determined, and the influence of atmospheric mixing or photochemistry can be quantified. Results of the three-dimensional model study are compared and applied to the PEM-West A hydrocarbon dataset, yielding a practical methodology for determining average OH concentrations and atmospheric mixing rates from the hydrocarbon measurements. Aircraft data taken below 2 km during wall flights east of Japan imply a diurnal average OH concentration of ~3 $\times 10^6$ cm^{-3}. The characteristic time for dilution with background air is estimated to be ~2.5 days for the two study areas examined in this work.

Introduction

An important objective of the PEM-West A experiment is to evaluate the anthropogenic impact to tropospheric chemistry over the Western Pacific Basin [*Hoell et al.*, this issue]. To achieve this objective, a key prerequisite is to characterize anthropogenically induced chemical signatures in the marine atmosphere. Characterizations based on air mass trajectories [*Gregory et al.*, this issue; *Talbot et al.*, this issue], lidar observations of ozone and aerosols [*Browell et al.*, this issue], and in situ hydrocarbon ratios [*Smyth et al.*, this issue] represent three independent bases for analysis. While the approach taken by Browell et al. relies on a quasi-statistical analysis of remotely sensed and in situ measurements, the other two approaches relate in situ observations to either the time from nearest anthropogenic contact (i.e., continental contact) or the degree of atmospheric processing determined from hydrocarbon ratios. The dependence of a particular in situ hydrocarbon ratio to time from emission is therefore an important link between the chemical signature approaches of Gregory et al. and Smyth et al. The report by *Talbot et al.* [this issue] establishes the relationship between the acetylene to CO ratio and time from the continent for a limited number of occurrences. However, from the observations and back-trajectory alone, it is not entirely clear how to interpret this relationship or discern the processes that affect the hydrocarbon ratios. By utilizing the results of three-dimensional photochemical model simulations, this study represents an attempt to distinguish the separate effects of photochemistry and atmospheric mixing on the hydrocarbons measured during PEM-West A and back-trajectory information.

[1]Aeronomy Laboratory/NOAA, Boulder, Colorado

[2]Also at Cooperative Institute for Research in Environmental Sciences, University of Colorado, Boulder, Colorado

[3]Georgia Institute of Technology, Atlanta, Georgia

[4]Atmospheric Sciences Division, NASA Langley Research Center, Hampton, Virginia

[5]Department of Chemistry, University of California, Irvine, California

Paper number 95JD02733.
0148-0227/96/95JD-02733$05.00

Anthropogenic hydrocarbons are perhaps the most convenient in situ chemical species to indicate anthropogenic activity, since they are usually emitted directly from combustion, leakage, or solvent applications. Based on kinetic measurements and model studies, the OH molecule has been determined to be the dominant agent in the initial oxidation of CO and most hydrocarbons [*Levy*, 1971; *Logan et al.*, 1981]. Seasonal differences in C_2-C_4 hydrocarbon ratios at a remote Canadian site have also been shown to be consistent with OH oxidation as their dominant photochemical destruction mechanism [*Blake and Rowland*, 1986; *Jobson et al.*, 1994]. Given the atmospheric importance and difficulty in determining OH concentrations accurately, it is tempting to use hydrocarbon measurements to infer average OH concentrations. Several studies have attempted to do this, using hydrocarbon observations and their different reactivities to OH for urban [*Calvert*, 1976; *Singh et al.* 1981; *Blake et al.*, 1993], rural [*Roberts et al.* 1984], and free-tropospheric [*Bamber et al.*, 1984; *McKenna et al.*, 1995] air masses. In most of these studies the ratios of reactive hydrocarbons to a relatively inert hydrocarbon are assumed to be due entirely to OH photochemistry, implicitly assuming that transport and dilution effects are removed within the ratioing operation. However, the need to also consider background hydrocarbon levels for relatively clean situations [*McKenna et al.*, 1995] and interactions between photochemistry and atmospheric mixing close to emission sources [*McKeen et al.*, 1990] are important caveats related to this hydrocarbon ratio approach.

Hydrocarbon ratios have also been used as a measure of "photochemical age" of an air mass [*Nelson and Quigley*, 1982; *Roberts et al.*, 1984, 1985; *Rudolph and Johnen*, 1990]. *Parrish et al.* [1992] made an extensive compilation of available data on simultaneous measurements of ethane, propane, and butane over several parts of the world. By plotting the ratio of n-butane to ethane against the ratio of propane to ethane, they were able to obtain a surprisingly consistent relationship between the two ratios. However, this relationship did not follow what was expected from pure OH kinetics alone. Using three-dimensional model calculations, *McKeen and Liu* [1993] explained this deviation in terms of the effects of atmospheric mixing with background air on the hydrocarbon ratios and the relationship between the two ratios. There are two general conclusions from the McKeen and Liu study that can be tested or utilized in the interpretation of the PEM-West A hydrocarbon data. First, atmospheric mixing has a profound effect on not just the concentration of an individual hydrocarbon but certain hydrocarbon ratios as well. Secondly, additional information, such as back-trajectory analysis, is necessary to separate out the individual effects of photochemistry and atmospheric mixing. In this sense, observed hydrocarbon ratios by themselves are indicators of the combined influences of photochemistry and atmospheric mixing.

This work represents an extension of the *McKeen and Liu* [1993] study to include the PEM-West A hydrocarbon observations. This dataset represents the largest collection of hydrocarbon data ever collected within a single intensive filed campaign prior to 1994. We first review several hydrocarbon relationships from the perspective of both the observations and the three-dimensional model results to illustrate the applicability of fitting procedures to derive meaningful information. The deviation of the hydrocarbon ratios from the kinetic-decay line reported by *Parrish et al.* [1992] is also evident in the PEM-West A aircraft observations and most easily explained by the influence of the large ethane background within the dilution process. By incorporating back-trajectory information within the three-dimensional model analysis, several important results are obtained. Within an idealized setting of the three-dimensional model, a simple technique is derived for determining the relative importance of photochemistry and dilution to the hydrocarbon ratio for a specific region of the model domain. This technique relies heavily on the simplified conceptual dilution model presented by *McKeen and Liu* [1993], which contains some inherent limitations that must be addressed before the practical extension of this technique can be applied to the observed data set. A limited subset of the PEM-West A data is used as a test application of the technique, from which atmospheric implications and comparison to the three-dimensional model results are discussed.

Model Calculations

The three-dimensional model used in this study is described by *Liu et al.* [this issue]. A more detailed description can be found in the work of *McKeen et al.* [1991]. Meteorological and physical variables derived from a three-dimensional, hydrostatic, compressible, primitive-equation model (more commonly called the Penn State/NCAR mesoscale model, version MM4) [*Anthes et al.* 1987] are used to drive a coupled photochemistry-transport model for the physical domain shown in Figure 1. A 17-day simulation (0000 UT, September 20, 1991, to 0000 UT, October 6, 1991) was chosen to correspond to the bulk of flight time (flights 6-13) in the vicinity of the Asian continent during the PEM-West A field experiment. Transport of individual species is accomplished by the upstream finite difference algorithm of *Smolarkiewicz* [1984] with one corrective step and cross terms included to reduce numerical diffusion. Horizontal and vertical diffusion, as well as vertical mixing within the convective boundary layer are also included as in the work of *McKeen et al.* [1991]. As mentioned by *Liu et al.* [this issue], there are some minor differences in the model structure and boundary conditions used in the PEM-West A version of the photochemical-transport model. Most importantly, convective transport due to cloud pumping is included as a transport process according to *Lin et al.* [1994], and boundary conditions above 5 km for several key species are set proportional to potential vorticity to better simulate the stratospheric influence on the free troposphere.

Details of the emissions inventory used within the three-dimensional photochemical model are outlined by *Liu et al.* [this issue]. Anthropogenic emissions of NO_x, which are necessary for the calculation of key photooxidants, are based on the spatial distribution of NO_x emissions for the western Pacific [*Dignon*, 1992] updated to 1988 annual estimates [*Kato and Akimoto*, 1992]. The emissions of CO and hydrocarbons are based on fuel use statistics for individual countries [*United Nations (UN)*, 1990], individual Chinese provinces [*State Statistical Bureau of China (SSBC)*, 1989], and emission ratios (relative to NO_x) for fuel usage categories determined by the Environmental Protection Agency [*Environmental Protection Agency (EPA)*, 1989]. All emissions are assumed to occur in the first model layer (~80 m thick), due to lack of information on the vertical partitioning of the emissions.

As explained by *McKeen et al.* [1991], the lumped hydrocarbon oxidation mechanism of *Lurmann et al.* [1986] is

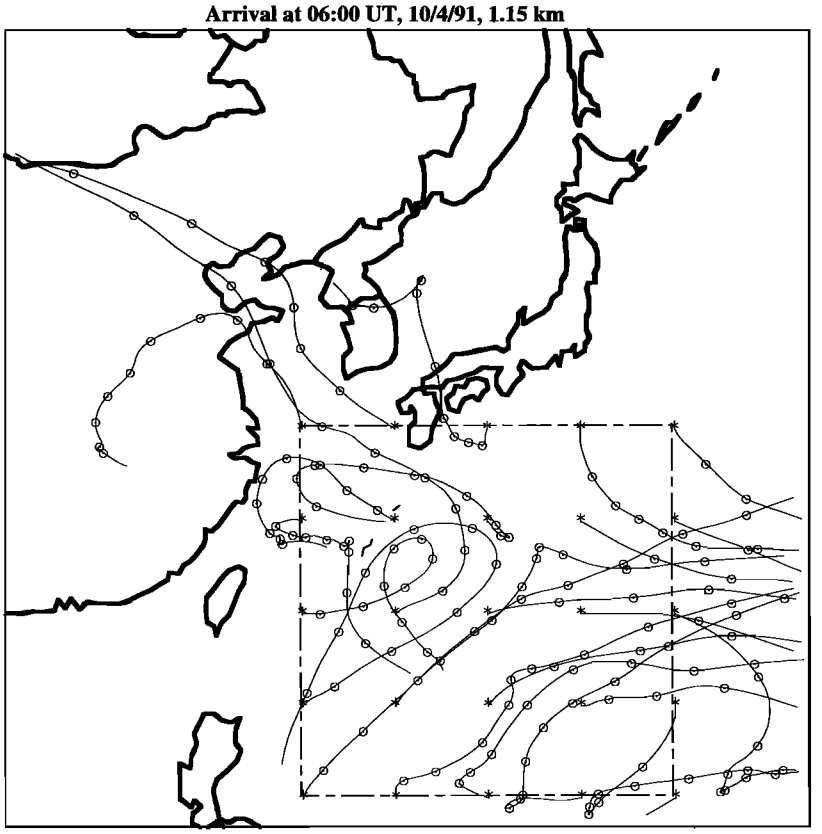

Figure 1. The three-dimensional mesoscale model domain and back trajectories determined for every fifth point (asterisks) at ~1.15 km altitude within the study area outlined by the dashed line. Circles along the trajectories are every 12 hours.

used in the full photochemical calculations. Each lumped hydrocarbon class is based on OH reactivity and may contain dozens of compounds. To simulate the individual hydrocarbons (HCs) measured during PEM-West A, OH values were saved at 0.5-hour intervals from the full photochemical run and used to calculate loss rates for CH_4, CO, C_2H_6, C_2H_2, C_3H_8, n-C_4H_{10}, and toluene within a separate calculation. These species are selected for their wide range of OH reactivities [*DeMore et al.*, 1992; *Atkinson*, 1990] as well as the numbers of observations above detection limits. Unlike the detailed photochemical calculations, the additional complication of inhomogeneous HC emission ratios (relative to CO) is removed for the specific HC simulations by assuming that emission rates are everywhere proportional to that of CO. Table 1 gives the emission ratio, boundary, and initial conditions for the individual HC. Emission ratios for the specific HC simulations were determined from the highest pollution measurements during PEM-West A [*Blake et al.*, this issue]. It is implicitly assumed in the emission ratio determination that all of the individual HC are emitted from a common anthropogenic source. In reality, this is not the case, particularly for CH_4, which has predominantly biogenic sources for this region.

It should be emphasized that the three-dimensional model formulation is inherently simplified to capture the individual effects of photochemistry and atmospheric mixing and is not designed for direct comparisons of model-simulated HC distributions with observations. Previous applications of the three-dimensional model have focused largely on photooxidants, including nitrogen oxides. Comparisons of model results to ground-based [*McKeen et al.*, 1991; *Trainer et al.*, 1993] and airborne measurements [*Lin et al.*, 1994; *Liu et al.*, this issue] have been successful in terms of predicting observations at a given point and time, as well as basic relationships between various photooxidants. From all indications the model system appears to adequately address transport and its interaction with oxidant photochemistry in the lower troposphere over timescales from ~1 hour to a few days and distance scales between ~150 and 3000 km. Thus the three-dimensional model results are well suited for examining the interaction between photochemistry and transport for the conditions of the PEM-West A experiment but not appropriate for direct comparison to observed HC, since absolute emission strengths over much of Asia are unknown.

We restrict the analysis of three-dimensional model and observed HC to the lowest 2 km of the troposphere for two

Table 1. Three-Dimensional Model Boundary Conditions, Emission Ratios Relative to CO and Photochemical Lifetimes (at 290°K, 0.87-atm pressure and OH =1.5 $\times 10^6$ cm^{-3})

Species	Bound. Condition	Emis. Ratio	OH Lifetime
CH_4	1708. ppbv	.25	3.9 yr
CO	70. ppbv	1.	33.9 day
C_2H_6	380. pptv	.0126	35.5 day
C_2H_2	44.1 pptv	.0087	10.9 day
C_3H_8	18.2 pptv	.01	7.8 day
n	7. $\times 10^{-6}$ pptv	.0068	3.2 day
Toluene	7. $\times 10^{-8}$ pptv	.0062	1.2 day

reasons. First, the focus of this study is on anthropogenic HCs which display highest concentrations close to the surface near urban sources [*Blake et al.*; this issue, *Gregory et al.*, this issue]. As discussed below, it is advantageous within the analysis to reduce uncertainties associated with assumed background concentrations by sampling air masses with clear anthropogenic signals. Secondly, although enhanced HC concentrations were observed at higher altitudes, particularly above 7 km, the likelihood that these air masses are a result of convective pumping introduces uncertainty as to their origin, which could be upwind of the model domain [*Liu et al.*, this issue]. Model boundary and initial values (Table 1) were adopted from measurements made below 3 km over remote oceanic areas during the PEM-West A mission. Table 1 also shows the expected lifetime of the chosen HC for a particular average OH concentration in the lower atmosphere ranging from ~1 day for toluene to ~4 years for CH_4. To help demonstrate the impact of photochemistry on the individual HC, seven additional species are also calculated with emissions, boundary and initial conditions identical to those listed in Table 1, but with photochemical destruction turned off. As shown below, relationships between these inert analogs provide useful information for diagnosing the three-dimensional model results and gaging the influence of photochemistry.

As discussed by *McKeen and Liu* [1993], an important element needed to unambiguously discern the effects of photochemistry versus atmospheric dilution is the time since emission of the HCs into the sampled air mass. To derive this quantity, for both model results and observations, back-trajectories are calculated isokinetically from the mesoscale model-derived half-hour three-dimensional wind fields, with three-dimensional mapping of grid centers to backward integrated origination coordinates saved at 2-hour intervals. Eight-point interpolation between grid centers is then used to map the trajectory for an arbitrary location, with the shortest time and location of land contact being determined to 2-hour and 60-km resolution. Because of uncertainty in the actual coastline with respect to the model grids, one grid square is added to the land use database, so that land contact here is defined as 60 km or less seaward from the actual coastline.

Model Results

This section is divided into two general parts. Section A discusses various HC relationships common to both the three-dimensional model and the observations. From this discussion the effects of atmospheric mixing within the PEM-West A observations will be demonstrated and quantified relative to the rate of OH photochemistry. Section B incorporates the back-trajectory analysis to establish a relationship between model-derived HC concentrations and time from emission. From the results of this section, a procedure for quantitatively determining the individual effects of photochemical decay and atmospheric mixing is derived and applied to a selected set of PEM-West A observations.

Section A, Basic Hydrocarbon Relationships

Although the three-dimensional model calculation extends over a large region of the eastern Asian continent, only a limited subdomain of the model is useful in simulating the conditions of the PEM-West A experiment. The region enclosed by the dashed lines in Figure 1 is chosen as the study area, and was chosen to coincide, as much as possible, with the study area of *Gregory et al.* [this issue]. The effects of direct emissions from the strong source regions are therefore eliminated, restricting the analysis to open-ocean conditions under various degrees of anthropogenic impact. Model data for a single time period (0400 UT, October 4, 1991) is chosen for comparison. This day and the previous day were periods where moderately high pollution outflow from the Asian continent was simulated by the photochemical-transport model. The choice of a particular day is not important to the analysis, but October 4, 1991, provides a larger range of conditions that vary from moderately polluted to pristine.

As discussed by *Brost* [1988], regional scale three-dimensional photochemical models are limited to large extent by influence of boundary conditions, particularly as one goes higher in the free troposphere. Indeed, most of the three-dimensional model values within the southern and eastern halves of the subdomain shown in Figure 1 are determined by the model boundary conditions for flow conditions encountered throughout much of the 17-day simulation period and are essentially artifacts of the three-dimensional model formulation. Since the values determined by the boundary conditions are of little interest, only those points having previous land contact, as determined by model back-trajectory analysis, are considered. Figure 1 illustrates the back-trajectories near 1 km altitude for every fifth point within the model subdomain used in the analysis. Although most trajectories originate from the model boundaries at this height, there is a high percentage that originates from north of Shanghai, the China Sea, and the southern part of Japan.

To facilitate discussion of the interaction between atmospheric mixing and photochemistry, it is useful to consider a highly idealized conceptual model relating the two processes. In a very simplistic approach, the mixing ratio of emitted species X can be changed by chemical loss or mixing with an infinite reservoir of background air:

$$\frac{dX}{dt} = -L_X X - K(X - X^B) \tag{1}$$

where X is the mixing ratio, t is time, X^B is the prescribed mixing ratio of X in the background air, $L_X = k_x[OH]$ is the loss frequency of species X with OH (bimolecular reaction rate constant k_x) and K is a mixing coefficient used to parameterize all the processes that mix species X with background air. There are several major simplifications in equation (1) that limit its applicability. Most important is the fact that mixing with air masses containing mixing ratios of X other than the background value X^B is ignored. For inert species this is not a problem, since the mixing process is entirely linear, but the addition of photochemical loss disrupts this linearity, which cannot be addressed in equation (1). Additionally, applying this simple formalism to observed data leads to practical problems, in particular a very strong dependence of the assumed background mixing ratio for the less reactive hydrocarbons. We also must assume that K and L_X are constants in order to obtain the analytical solution

$$X = \frac{KX^B}{K+L_x} + \left(X^0 - \frac{KX^B}{K+L_x}\right) e^{-(K+L_x)t} \tag{2}$$

where X^0 is the initial mixing ratio of X upon emission.

The conceptual picture of air parcel aging embodied by equation (1) is specifically designed for an isolated source

embedded within a very large and relatively clean region, such as pollution plumes originating from islands or coastal locations. Since only photochemical decay and dilution are considered, the simple formulation would not apply to conditions where emissions or multiple sources are also influencing concentrations (e.g., a polluted continental boundary layer). Equation (1) offers a simple formulation that incorporates several concepts related to hydrocarbon aging. The HC aging picture based solely on OH photochemistry [e.g., *Roberts et al.*, 1984; *Rudolph and Johnen*, 1990] is augmented by the dilution term. *Smyth et al.* [this issue] use meteorological scaling arguments and an analogy to the concentration decay observed with exponential dilution flasks [*Lovelock*, 1961] to infer rough estimates of atmospheric dilution. The exponential decay within a dilution flask system is equivalent to equation (2) for an inert species with no background and the dilution constant K replaced by the flow velocity divided by the flask volume. The importance of background values [*McKeen and Liu*, 1993; *McKenna et al.*, 1995] and the qualitative argument of HC clock resetting by discrete mixing with air parcels of a different age [*Parrish et al.*, 1992] are implicitly incorporated within the continuous dilution term.

Species Versus Species Relationships

When a similar equation is written for species Y, ratios can be derived from equation (2) that are independent of time and/or the mixing parameter K, depending on assumptions specific to each HC. For example, if species X and Y are inert, their ratio to the amount above background is a constant and equal to the emission ratio $(X^0-X^B)/(Y^0-Y^B)$. Similarly, if the photochemical decay rates ($L_{X,Y}$) are much larger than the mixing parameter K, time can be eliminated between the two solutions, yielding a linear photochemical decay on a log-log plot. Figures 2a and 2b show the limiting cases for the dilution of inert species (solid line) and the photochemical OH-kinetic relationship (dashed-dotted line) for the C_3H_8 - n-C_4H_{10} pair. The placement of the intersecting point in both of these figures is somewhat arbitrary, but the observed and three-dimensional modelled data clearly fall between these two limiting cases. A general solution of Y versus X, including both photochemical and background terms, has a complicated dependence on the assumed initial mixing ratio as well as background conditions. If the two species have photochemical loss rates strong enough to assume that background concentrations are zero, then the relationship simplifies to

$$X = X^0\left[\frac{Y}{Y^0}\right]^{\frac{K+L_X}{K+L_Y}} \quad . \tag{3}$$

The slope of a log-log plot of two such species will yield the exponent in this equation. Since L_x and L_y are related by a known constant, the relative quantity K/L_y may be derived. Although the regression procedure does not allow an absolute estimation of [OH] or dilution rates, it is interesting to apply the simple relationship expressed in (3) to the PEM-West A data set to examine, in a mean or average sense, the relative contribution of dilution and photochemistry. The

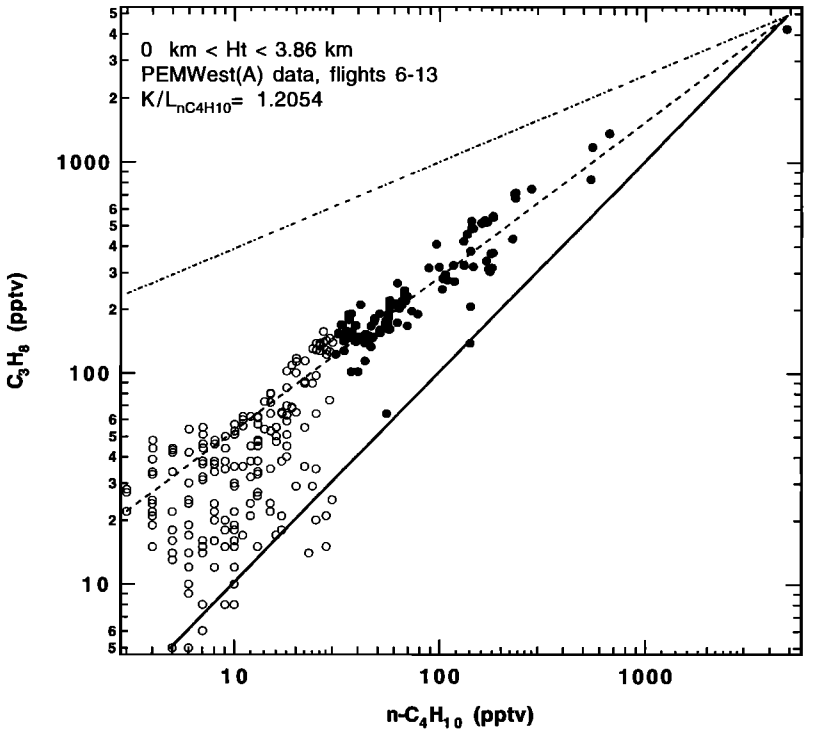

Figure 2a. Correlation plot of observed C_3H_8 versus n-C_4H_{10} during flights 6-13 of PEM-West A. Only data collected at less than 3.9 km altitude are shown. The solid line denotes the expected relationship based on only dilution of inert species. The dashed-dotted line is the relationship based on OH reaction kinetics only. The dashed line is the regression fit through the data when n-C_4H_{10} is greater than 30 pptv (solid circles). The intersection of the lines is arbitrary, defined by the highest n-C_4H_{10} point along the abscissa and the regression fit at this point.

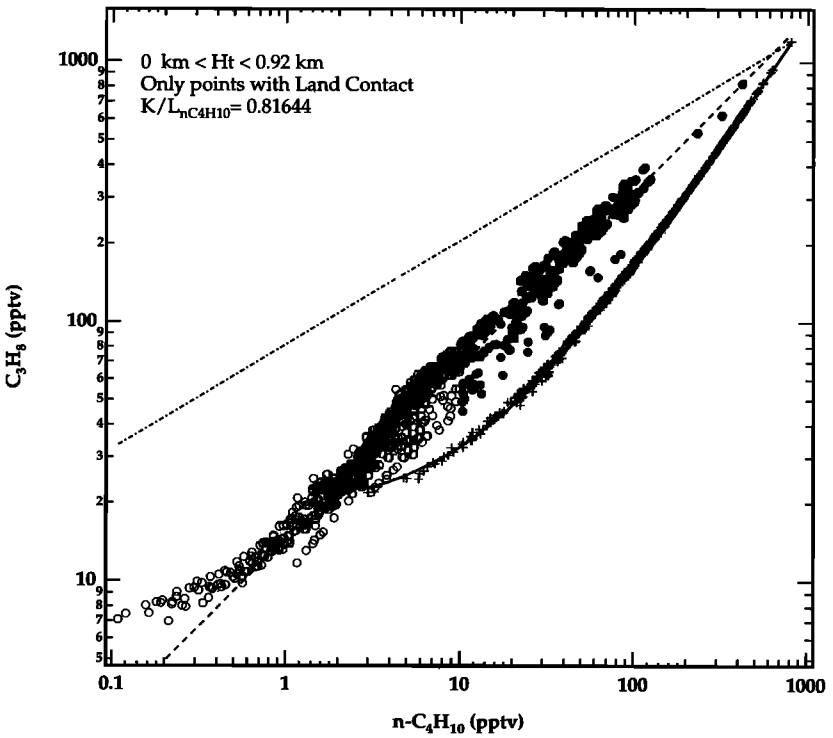

Figure 2b. Correlation plot of C_3H_8 versus n-C_4H_{10} from the three-dimensional model results. The lines have the same meaning as in Figure 2a, except the dashed line is the regression fit for n-C_4H_{10} points greater than 10 pptv. Model results for the inert analogs to C_3H_8 and n-C_4H_{10} are shown by pluses. Only three-dimensional model points determined to be over land within the previous 15 days are shown.

multiplicity of possible reactive HC regressions allows a consistency check for both the model-generated and the observed data sets.

Figure 2a shows the n-C_4H_{10} versus C_3H_8 correlation plots for the PEM-West A observations during flights 6 through 13 below 4 km altitude, along with the best fit line determined by least squares regression. However, we restrict the n-C_4H_{10} data used in slope determinations to greater than 30 pptv (97 points) due to a significant amount of scatter in the correlation with other alkanes when n-C_4H_{10} is less than 30 pptv. Although C_3H_8 was always measured above detection limit and may therefore have a significant background concentration, the 30 pptv limit on the n-C_4H_{10} forces the accompanying C_3H_8 to be well above a nominal background value. Thus by restricting the analysis to the most polluted samples, one may assume that the C_3H_8 background is negligible, and equation (3) is applicable for the C_3H_8 versus n-C_4H_{10} regression within Figure 2a. The regression of the points with n-C_4H_{10} > 30 pptv in Figure 2a yields a slope of 0.73 ±0.03. If n-C_4H_{10} is chosen as the reference species, the relative term $K/L_{n\text{-butane}}$ from this regression becomes 1.2 ±0.27. This number implies that the concentration changes of hydrocarbons with reactivities less than or equal to n-butane over the western Pacific are influenced equally or slightly more by dilution than by photochemistry. The results are quite similar when comparing other highly reactive alkanes to C_3H_8. Again, using the OH reactivity with n-C_4H_{10} as a reference, the dilution coefficient to loss ratio ($K/L_{n\text{-butane}}$) determined from regression slopes of i-C_4H_{10}, n-C_5H_{12}, i-C_5H_{12}, and n-C_6H_{14} are 1.14, 1.30, 0.93 and 1.27, respectively. As the reactivity increases, the uncertainty becomes larger because there are fewer points measured above detection limit and even fewer points with mixing ratios above the n-C_4H_{10} discrimination limit of 30 pptv (e.g., 67, 35, 41, and 5 points for i-C_4H_{10}, n-C_5H_{12}, i-C_5H_{12}, and n-C_6H_{14}, respectively). Using n-C_4H_{10} or i-C_4H_{10} as the least reactive HC in the regression determination also yields quite similar results (equivalent $K/L_{n\text{-butane}}$ = 1.2 ±0.4) but with additional uncertainty due to fewer points and the smaller difference between the mixing slope of 1 and the photochemical slope between the more reactive alkanes. The highly reactive alkanes therefore yield a reasonably consistent value of the relative importance of dilution and photochemistry, regardless of the choice of HC used in the regressions.

Figure 2b illustrates the correlation plot between C_3H_8 and n-C_4H_{10} for the three-dimensional model results with the corresponding relationship between inert analogs also shown. Notice that the inert species follow the linear dilution curve almost exactly. To be consistent with the treatment of the observations, only data pairs with n-C_4H_{10} > 30 pptv should be used in the regression. However, the three-dimensional model does not display large scatter below any n-C_4H_{10} value, and better statistics are obtained by using a lower cutoff for the model data. From the correlation of points in Figure 2b, $K/L_{n\text{-butane}}$ assumes a value of 0.80 ±0.1, 0.82 ±0.06 and 0.79 ±0.02 for n-C_4H_{10} cu-off values of 30, 10, and 0.6 pptv, respectively. We therefore apply the 10 pptv n-C_4H_{10} cut-off criteria for the model data in the following analysis. Although the effect of the imposed 18 pptv C_3H_8 model boundary condition is obvious in Figure 2b at the lowest concentrations for both the reactive and the inert model cases, the regression to equation (3) requires negligible background contribution.

The final result is not too sensitive to the assumption of negligible C_3H_8 background; for example, for a n-C_4H_{10} cutoff value of 10 pptv the ratio increases 12% if the correlation is redone with the term $K[C_3H_8]^B/(K+L_{propane})$ in equation (2) assumed to be 10 pptv rather than zero.

Figures 2a and 2b therefore illustrate the usefulness of the HC relationships in obtaining a quantitative handle on the relative importance of photochemistry and dilution as well as the consistency between the three-dimensional model results and the observations. Knowing that the dilution process on the average is occurring as rapidly as solstice n-C_4H_{10} oxidation has implications in terms of interpreting various HC and oxidant relationships in the lower troposphere. For example, from the dilution flask analogy *Smyth et al.* [this issue] estimate that photochemistry contributes ~25% to the variation of the C_2H_2/CO ratio over the western Pacific. Since the C_2H_2/CO ratio has a characteristic photochemical lifetime ~5 times longer than n-C_4H_{10}, our analysis suggests that on the average, photochemistry accounts for ~17% of the C_2H_2/CO variation. The two estimates are therefore quite similar and consistent with the highly efficient dilution inferred from the comparison of C_2H_2/CO ratios to the isentropic back-trajectory air mass classification scheme [*Smyth et al.*, this issue; *Merrill et al.*, this issue]. Because dilution is apparently so effective for the PEM-West region, our results generally imply that the use of hydrocarbon ratios as photochemical markers, or as indices of reaction time, should only be applicable when the hydrocarbons are more reactive than n-C_4H_{10}. Additionally, the high reactivity of these HC requires either sampling of very polluted conditions or extremely sensitive and accurate measurements under less polluted conditions in order to accurately use them as photochemical clocks. Ratios of less reactive species still provide a measure of atmospheric processing, but changes in a HC ratio are influenced more by physical mixing than by photochemistry. Lastly, rough estimates of K can be derived for reasonable assumptions of [OH]. From the three-dimensional model, a diurnally average OH concentration of 2 $\times 10^6$ cm^{-3} is determined over the study area outlined in Figure 1 between the surface and 1 km, yielding a mean lifetime due to dilution of ~2.4 days for the model results and 1.8 days for the observations. *Crawford et al.* [this issue] use a detailed box-model analysis to estimate an average lower tropospheric [OH] concentrations of 1.5 $\times 10^6$ cm^{-3}, corresponding to a dilution lifetime derived from the observations of 2.4 days. Considering the 30% uncertainty between the two OH estimates and the 30% uncertainty in the observed $K/L_{n\text{-butane}}$ determination, the dilution rates determined from the three-dimensional model and observed data sets can be considered nearly the same.

Figures 3a and 3b show the correlation plots of C_2H_6 versus C_3H_8, illustrating the effect of a significant background on the relationship between two HC. The boundary conditions and emission ratios for both the reactive species and the inert analogs are taken from Table 1 for the three-dimensional model results in Figure 3b. Although general analytical solutions relating two such HC can be derived, they depend on the assumed background, which is undefined. There may exist a unique set of background concentrations that would yield a meaningful regression analysis from the observed data. However, such an exercise may overstate the validity of the simple dilution model, especially for measurements over a region as large as the western Pacific where a background may have strong latitudinal and temporal dependencies. Comparing Figures 2a and 3a, there also appears to be a much tighter correlation between C_3H_8 and n-C_4H_{10} than between

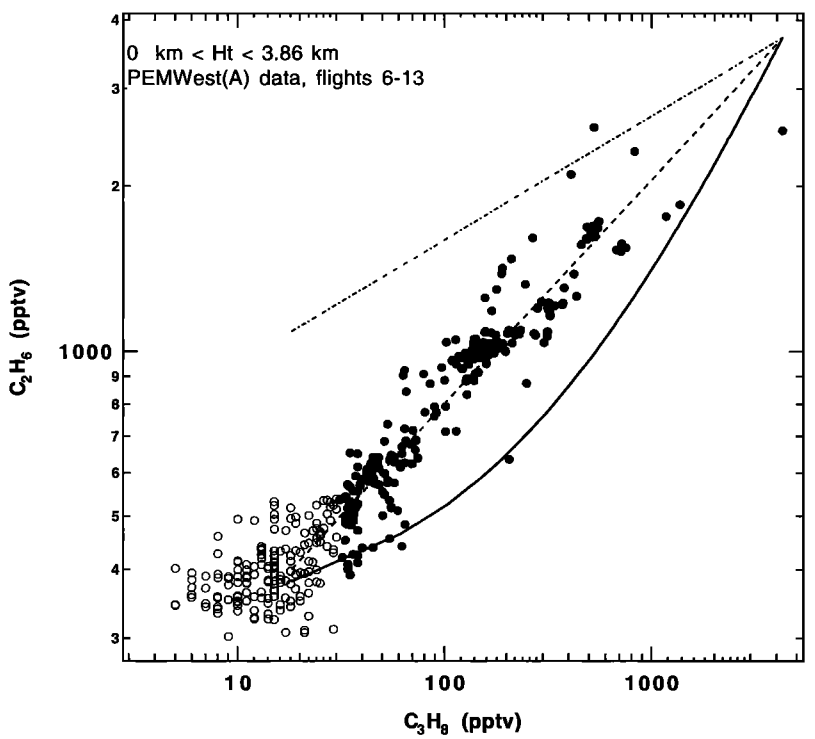

Figure 3a. Correlation plot of observed C_2H_6 versus C_3H_8 during flights 6 through 13 of PEM-West A. The lines have the same meaning as in Figure 2a.

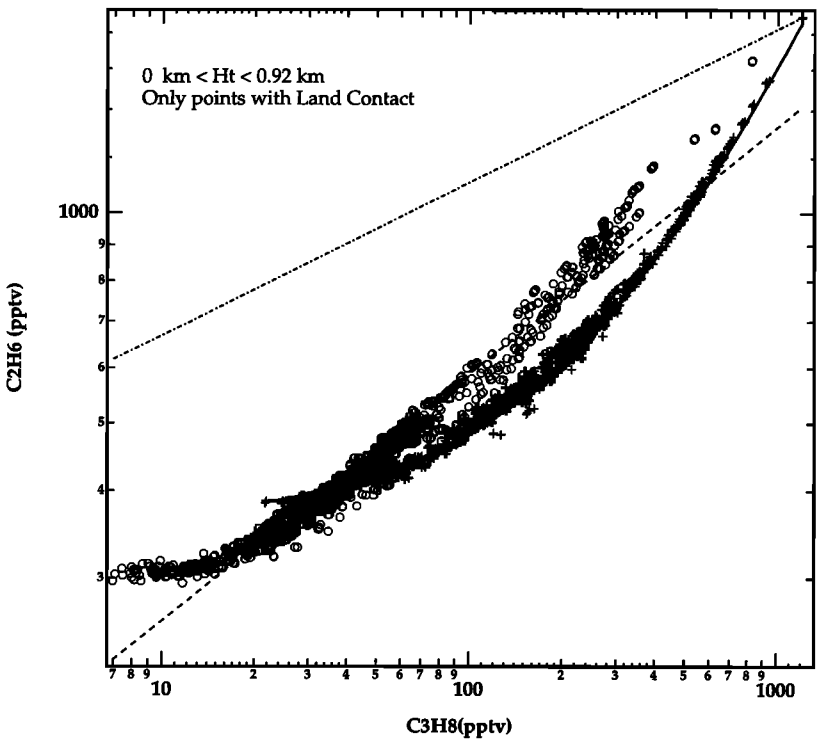

Figure 3b. Correlation plot of C_2H_6 versus C_3H_8 from the three-dimensional model results. The lines have the same meaning as in Figure 2a.

C_2H_6 and C_3H_8 at the highest observed values. *Blake et al.* [this issue] discuss specific hydrocarbon fingerprints from individual flights and back-trajectory analysis. The tight correlation between C_3H_8 and n-C_4H_{10} would be consistent with a single source influencing all the measurements from the various sampling locations, while the stronger variations between C_2H_6 and C_3H_8 would suggest more heterogeneous emission patterns between source regions. One explanation for this discrepancy would be the influence of photochemistry biasing the result of the most recent source of emissions for the more reactive HC, while less reactive HC such as C_2H_6 are more likely to be influenced by multiple sources, over a larger region with differing emission fingerprints. Additional three-dimensional model runs that include a more complete and accurate accounting of heterogeneous emissions would be necessary to confirm this hypothesis. However, the three points in Figure 3a with high C_2H_6 to C_3H_8 ratios originated from eastern China [*Blake et al.*, this issue] as opposed to samples with lower ratios originating from Japan or South Korea. This would be consistent with a larger, continental source region influencing the C_2H_6 observations, as opposed to reactive HC concentrations which may be weighted more heavily toward a specific emission source closer to the coastline.

Figure 3b illustrates some inherent limitations of the regional three-dimensional model in describing the observed HC relationship in Figure 3a. While the inert analogs follow the dilution line closely, the same boundary and emission conditions lead to a displacement of the apparent background values for the reactive species. For example, the lowest values of the reactive C_2H_6 and C_3H_8 in Figure 3b approach 300 and 10 pptv, respectively, in contrast to the imposed boundary conditions of 380 and 18 pptv. Thus for the three-dimensional model to adequately approximate the observed background for moderately reactive HC, the boundary conditions in Table 1 would have to be adjusted on a species-by-species basis. Similarly, the sharp tailing-off of C_2H_6 in Figure 3b is an artifact of the limited domain and the boundary conditions, not evident in the observations. On the other hand, Figures 2b and 3b show the effect of chemistry on the HC relationships. The reactive species relationships show more scatter, due to different photochemical and mixing histories of individual air masses, as mentioned previously. In both figures the relationship between reactive species remains similar to the relationship for the inert species but are shifted to lower concentrations. The effect of chemistry thus appears to smear the basic relationship curve and also to displace the points as well as the backgrounds nearly along the strictly photochemical decay slope represented by the dashed-dotted line in Figure 3b. This implies that the mixing process dominates the C_2H_6 - C_3H_8 relationship, while the first-order effect of chemistry is simply to displace the background.

Ratio Versus Species Relationships

With a little algebraic manipulation of equation (2), similar relationships for the two limiting cases can be derived between an HC species and the ratio of two HCs. For the inert species

$$X = Z^B\left(B^{X/Z} + E^{X/Z}\frac{(Y/Z - B^{Y/Z})}{(E^{Y/Z} - Y/Z)}\right)$$

where $E^{I/Z}$ is the emission ratio of species I to species Z and $B^{I/Z}$ is the ratio of the background value of species I to that of species Z. For the other limiting case where $L_{X,Y,Z} >> K$, a linear slope on a log-log plot again defines the photochemical decay relationship. As in the case for one HC versus another, the general solution for the case of both dilution and

photochemistry being significant is complicated by a nontrivial dependence on initial conditions and the assumed background concentration, but the restrictive use of highly reactive HC (with zero assumed background) leads to a workable relationship between a species and a ratio:

$$X = X^0\left[\frac{Y}{Z}\frac{Z^0}{Y^0}\right]^{\frac{K + L_X}{L_Y - L_Z}}.$$

The slope of X versus Y/Z on a log-log plot again defines the exponent term which can be related to the loss rate of n-C_4H_{10}. It is easy to show that if Y and X are the same species, then the regression slope determined from the log(X/Z) versus log(X) yields the exact same result as simply determining the regression slope from log(X) versus log(Z), so there is no additional information obtained by examining n-C_4H_{10}/C_3H_8 versus n-C_4H_{10} for example. Figure 4a shows the limiting cases, observations, and best fit line for n-C_4H_{10}/C_3H_8 versus C_3H_8. As before, only samples in which n-C_4H_{10} is > 30 pptv are used in the regression fit. The regression slope yields a $K/L_{n\text{-butane}}$ ratio of 2.1 ±.5, nearly twice as large as previously determined.

Figure 4b shows the same relationship derived from the three-dimensional model results, which displays characteristics similar to that of Figure 4a. There is much more scatter to this relationship in comparison to Figures 2a and 2b; the best fit lines pass well below the highest point. The model $K/L_{n\text{-butane}}$ ratio (1.12 ±0.08) is likewise overpredicted by the three-dimensional model results in comparison to the ratio derived from the log(C_3H_8) versus log(n-C_4H_{10}) correlation derived in the previous section. Within the three-dimensional model, the larger scatter is due to emissions from different locations having different C_3H_8 values upon emission. The limiting case line corresponding to the inert species defines the relationship upon emission, with smaller emissions occurring at lower C_3H_8. The separated distribution of points in Figure 4b that are above the main line of scatter for 50 < C_3H_8 < 300 pptv are from Okinawa, which has relatively week emissions in comparison to the main HC sources to the north and east within the model runs. These points begin their decline toward lower values from a point shifted well above the main grouping, contributing to the scatter located above the regression line. Two of the three outliers for the observations shown in Figure 4a near C_3H_8 = 100 pptv are from flight 12 at low altitude over the Taiwan coast, which would confirm this explanation. However, *Blake et al.* [this issue] also point out that natural gas usage in Taiwan has a n-C_4H_{10} content relatively higher than the rest of eastern Asia. The worst outlier is from a sample collected 600 km east of Japan at 2 km and was determined from back-trajectory analysis to have originated ~100 km south of Tokyo 28 hours previously. The n-C_4H_{10} value for this point appears to be anomalous, although a complete absence of photochemistry for this single point could also explain the departure. Relative to Figures 2a and 2b, Figures 4a and 4b display much more scatter, primarily because there is a much larger separation between the photochemical and dilution limits. Spatial differences in emission ratios, photochemical loss, and mixing histories are more obvious, and influence regression fits by smearing the more constrained correlations shown in Figures 2a and 2b. When toluene/n-C_4H_{10} versus n-C_4H_{10} is compared in the three-dimensional model, even a higher degree of scatter is observed than in Figure 4b, suggesting that the time of

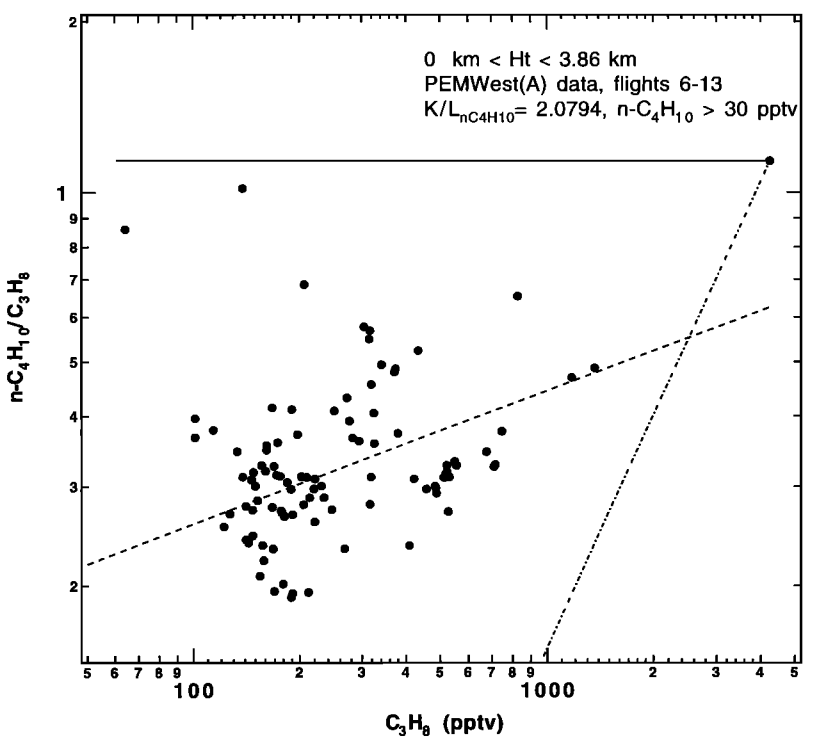

Figure 4a. Correlation plot of observed n-C_4H_{10}/C_3H_8 versus C_3H_8 during flights 6 through 13 of PEM-West A. The lines have the same meaning as in Figure 2a. The intersection of the photochemical and dilution lines is arbitrary and placed at the extreme value. The solid line, denoting dilution of the inert analogs, assumes a C_3H_8 background of zero.

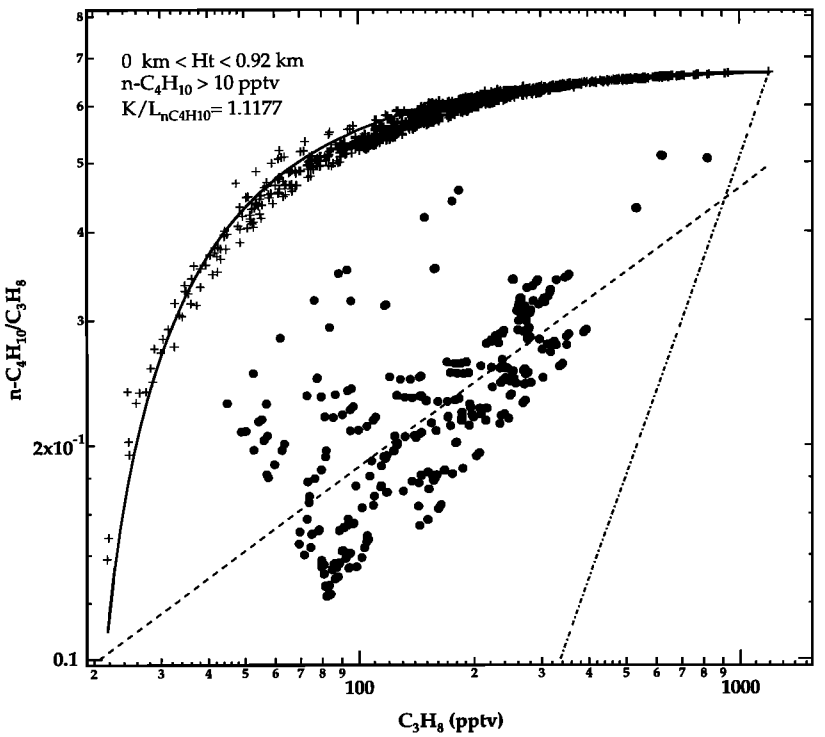

Figure 4b. Correlation plot of n-C_4H_{10}/C_3H_8 versus C_3H_8 from the three-dimensional model results. The lines have the same meaning as in Figure 4a. The solid line, denoting dilution of the inert analogs, assumes a C_3H_8 background given in Table 1.

emission relative to the diurnal OH pattern will also introduce scatter for very reactive HC with lifetimes less than a couple of days. This emphasizes the fact that the regression fits are intended to represent an ensemble average, while very different rates and interactions are occurring locally. Notice that forcing the three-dimensional model and observed regression lines in Figures 4a and 4b to fall on the extreme high point would increase the regression slopes and yield dilution to photochemical loss ratios closer to those determined from the species-species relationships but with high scatter about the regression line. This suggests that HCs or HC ratios used in a regression analysis should be chosen to have reasonable separation between the photochemical and inert-dilution limits; however, too much separation defeats the validity of the regression.

Figures 5a and 5b are similar plots for C_3H_8/CO versus C_2H_6, illustrating the effect of a significant background on the relationship. Since the species in the relationship are less reactive and have significant backgrounds, Figure 5b shows much less scatter than Figure 4b. Figure 5a also shows much more scatter compared to Figure 5b, which can simplistically be ascribed to variations in relative emissions between the three species that are not included in the three-dimensional model. The sharp tailing-off of the model results, an artifact of the imposed boundary conditions, is not apparent in the observations. Clearly, the regional scale model is an inappropriate tool for studying relationships between long-lived HC, particularly for clean conditions. As in the species-species relationships, the three-dimensional model results for the inert species follows the simplified mixing form quite well in Figures 4b and 5b. The reactive points are smeared compared to the inert relationship but preserves the essential shape. Similar to the discussion related to Figure 3b, the main effect of chemistry in Figure 5b is to shift the inert mixing relationship nearly along the photochemical decay slope.

Ratio Versus Ratio Relationships

The final comparison between HC relationships involves plots of one HC ratio versus another HC ratio. *McKeen and Liu* [1993] presented the two limiting cases and also the three-dimensional model results for n-C_4H_{10} over C_2H_6 versus C_3H_8 over C_2H_6 in relation to the observations reported in *Parrish et al.* [1992] and *Rudolph and Johnen* [1990]. Figures 6a and 6b show the observed data relationship and the three-dimensional model results for the same species. The "dilution line" assumes zero background values for n-C_4H_{10} and C_3H_8 but not for C_2H_6. The intersection of the lines corresponding to the two limiting cases is only significant for the three-dimensional model results and defines the emission ratios prescribed in Table 1. The relative position of the points and regression slope of Figure 6a is quite consistent with the data set presented by *Parrish et al.* [1992]. As discussed by McKeen and Liu, neither the observations nor the three-dimensional model results lie strictly along the photochemical decay or mixing lines but scatter in between. Moreover, since the relative location of a point with respect to the origin depends on the combined effects of photochemistry and mixing, there is no way to separate the two distinct effects from the HC relationships alone without knowing additional information, such as the time from emission. Within the three-dimensional model results of Figure 6b there appears to be two distinct population of points, and indeed the smaller grouping that lies above the main scatter is associated with the isolated

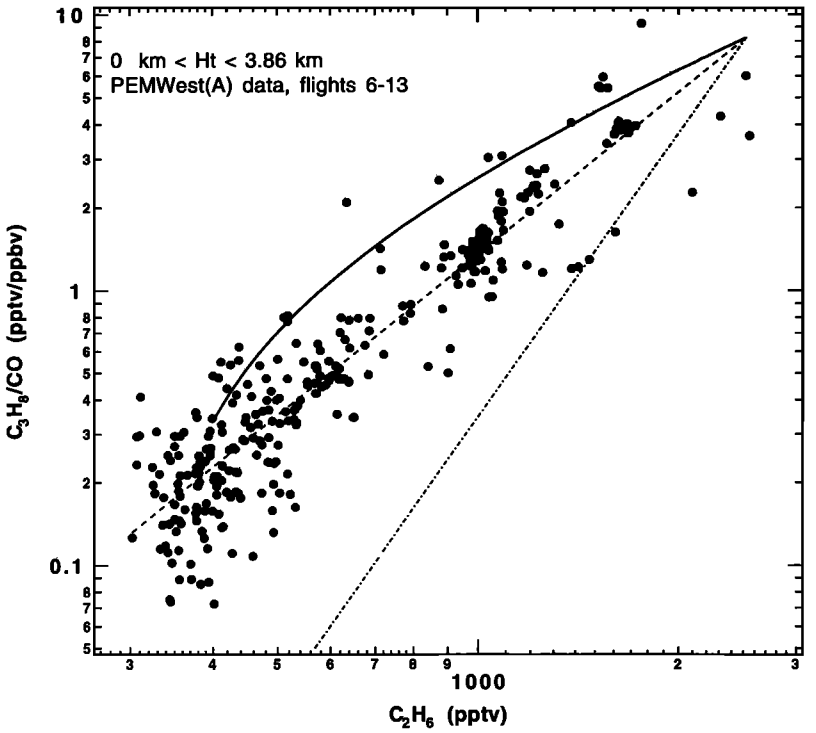

Figure 5a. Correlation plot of observed C_3H_8/CO versus C_2H_6 during flights 6 through 13 of PEM-West A. The lines have the same meaning as in Figure 2a. The intersection of the photochemical and dilution lines is arbitrary and placed at the extreme value.

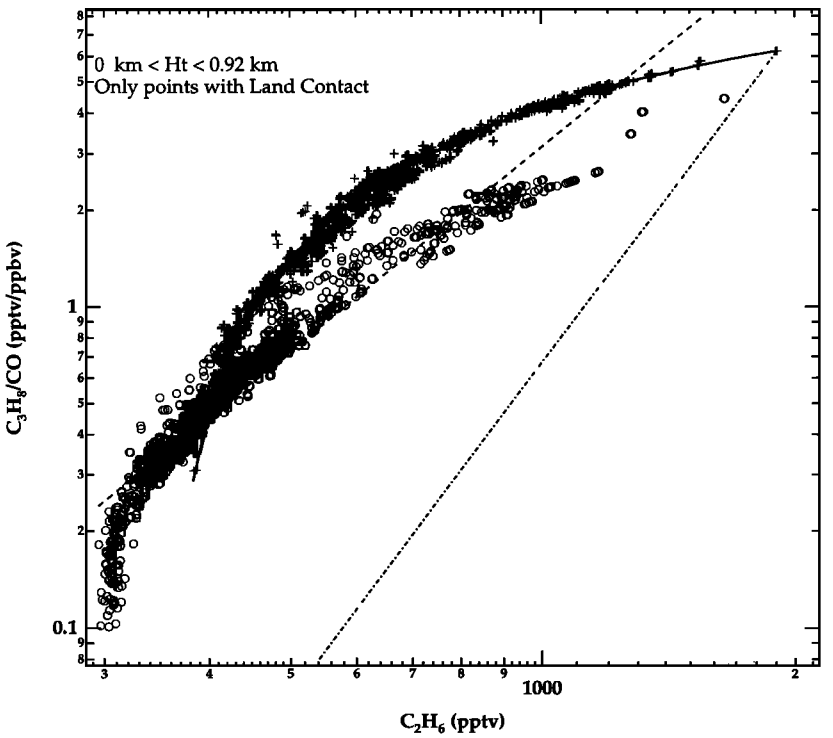

Figure 5b. Correlation plot of C_3H_8/CO versus C_2H_6 from the three-dimensional model results. The lines have the same meaning as in Figure 4a.

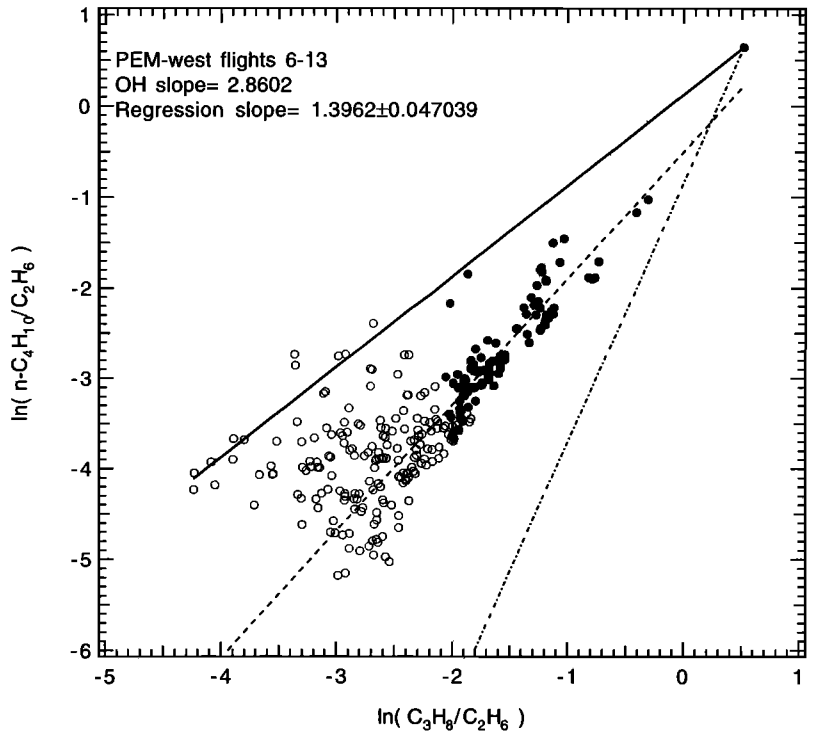

Figure 6a. Correlation plot of observed n-C_4H_{10}/C_2H_6 versus C_3H_8/C_2H_6 during flights 6 through 13 of PEM-West A. The lines and markers have the same meaning as in Figure 2a. The intersection of the photochemical and dilution lines is arbitrary and placed at the extreme value. Zero background is assumed for n-C_4H_{10} and C_3H_8 in the dilution line.

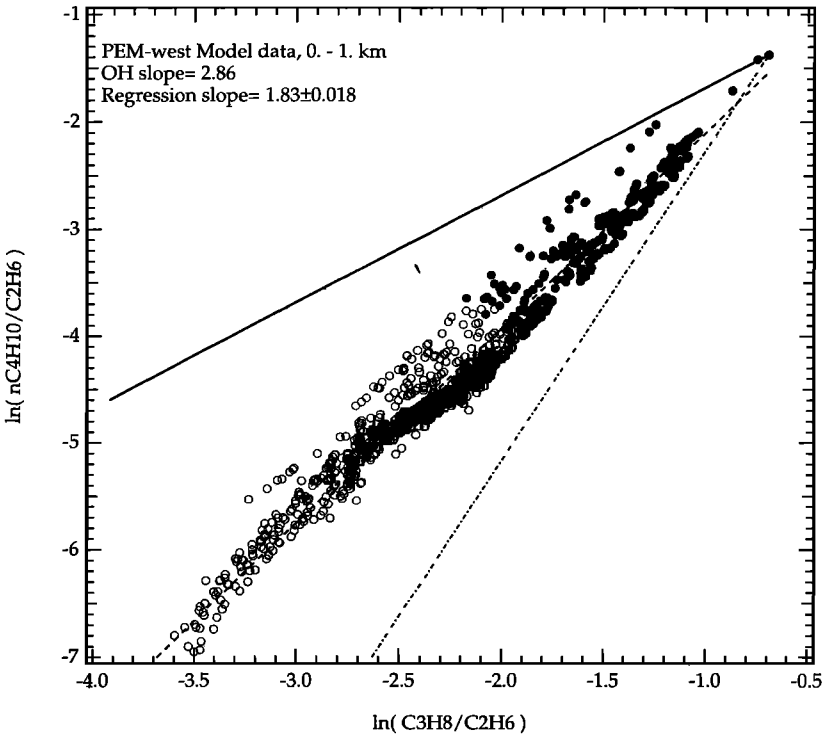

Figure 6b. Correlation plot of n-C_4H_{10}/C_2H_6 versus C_3H_8/C_2H_6 from the three-dimensional model results. The lines and markers have the same meaning as in Figure 2b. Zero background is assumed for n-C_4H_{10} and C_3H_8 in the dilution line.

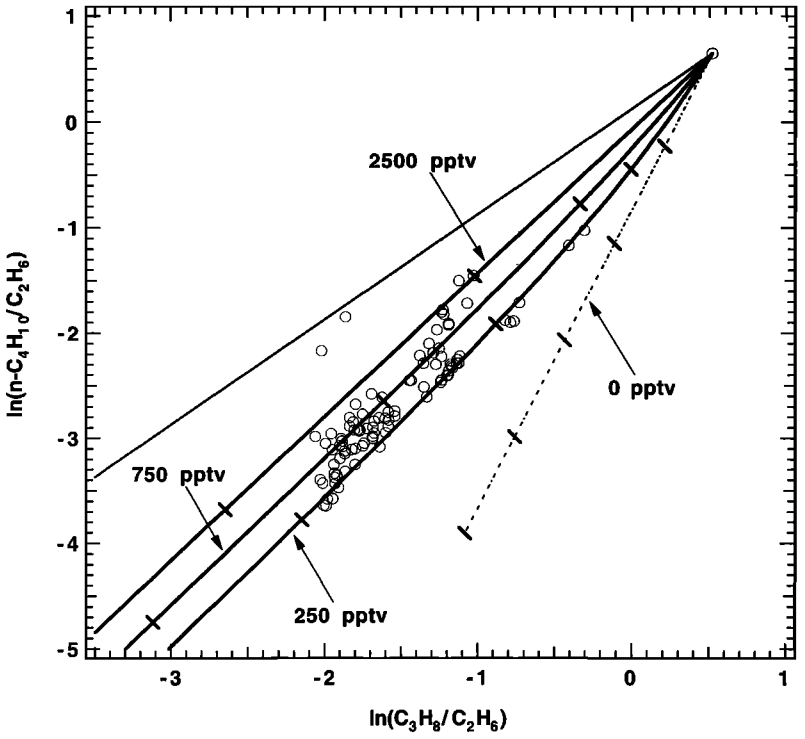

Figure 6c. Same as Figure 6a, except observations with n-C_4H_{10} > 30 pptv are shown as circles. Also shown are calculated curves (ratios derived from equation (2)) for different scaled C_2H_6 backgrounds. The 0 pptv case corresponds to pure OH photochemistry. A value of 1.2 is assumed for $K/L_{n\text{-butane}}$, and initial conditions are defined by the intersection point. Each tick along a curve corresponds to one n-C_4H_{10} lifetime due to OH reaction. See text for details.

Okinawa source. Thus an explanation of the scatter within Figures 6a and 6b would arise from the difference in HC decay between a point source emitting into relatively clean conditions and diluting rapidly, as opposed to a broad regional source with only peripheral contact with background air. However, the three-dimensional model OH concentration is higher within regional pollution plumes which also may contribute to the scatter.

As in the species-species and species-ratio relationships, the general solution to the ratio-ratio relationship when both background and photochemical loss are significant is dependent on background assumptions. However, unlike the previous cases the ratio-ratio relationship is not dependent on the absolute amount of HC upon emission, only the emission ratios. For the species used in Figures 6a, and 6b, the denominator has a significant background value and the numerators have negligible background values (with the appropriate windowing). In this case, manipulation of equation (2) for three species yields

$$\frac{X}{Y-\left(\frac{Y^B K}{K+L_Y}\right)} = C\left[\frac{Z}{Y-\left(\frac{Y^B K}{K+L_Y}\right)}\right]^{\frac{L_X-L_Y}{L_Z-L_Y}} \qquad (4)$$

where C is a constant dependent only on the emissions ratios of species X and Z with species Y. Thus if the background value Y^B is negligible, the slope of the regression line of the log of the ratios is exactly what would be expected from photochemical OH loss alone. If a background value of Y is well defined, then a similar regression line, with the denominator decreased by a scaled fraction of this background value, should yield the kinetic relationship. In the case that species Y is C_2H_6, this scaling fraction ($K/[K+L_Y]$) is ~0.9 when the dilution coefficient used in equation (2) is 1.2 times the n-C_4H_{10} photochemical lifetime, as derived previously. The shift of the observed data away from the photochemical line in Figures 6a and 6b is therefore explained by the simple dilution model to be due to an offset in the denominator, introduced by the C_2H_6 background. This is best illustrated in Figure 6c, which plots the ratios obtained from equation (2) assuming zero background for n-C_4H_{10} and C_3H_8 but four different scaled backgrounds for C_2H_6. In the solutions of equation (2) the initial concentrations of n-C_4H_{10}, C_3H_8, and C_2H_6 are 4.8, 4.24, and 2.5 ppbv, respectively, corresponding to the highest values observed near Yokota airport. The dilution coefficient to n-C_4H_{10} loss ratio ($K/L_{n\text{-butane}}$) is assumed to be 1.2, as deduced from the previous species-species analysis, and the individual curves are calculated with the independent variable being a multiple of the n-C_4H_{10} lifetime, as denoted by the tick marks along the parametric curves in Figure 6c. Most of the observed data points fall within the limits of 250 and 750 pptv assumed for the scaled C_2H_6 background. The two outliers near the inert-dilution line correspond to the samples taken directly over southern Taiwan, as mentioned above.

Figure 6c illustrates several important features of the simple dilution model and how the ratio-ratio relationship of these three particular species is explained by this model. The time increments along each curve illustrates the effect of increasing higher backgrounds on the rate of change of the ratio-ratio relationship. It is quite apparent that the background values not only affect the slopes of the ratio-ratio

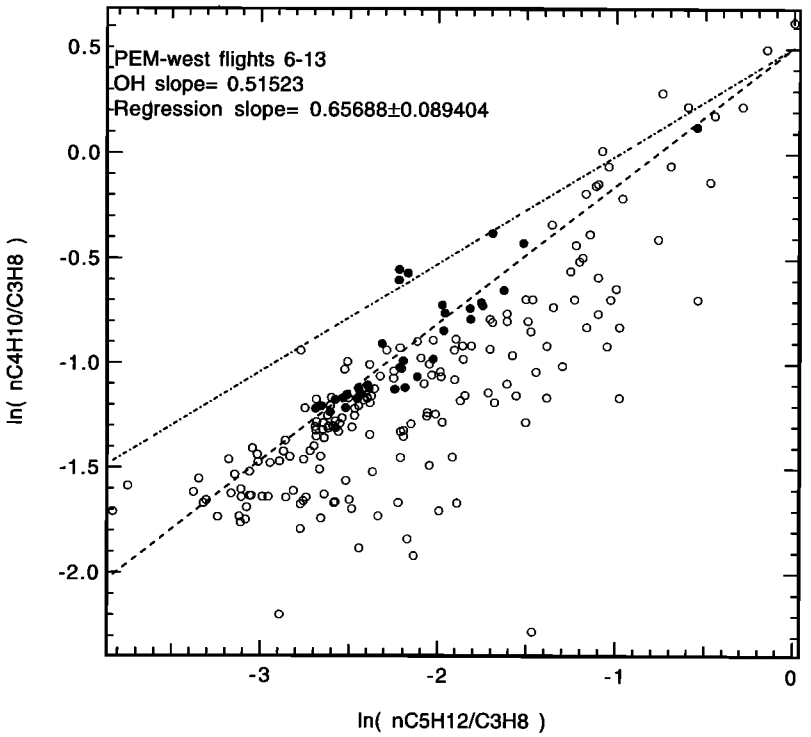

Figure 7. Correlation plot of observed n-C_4H_{10}/C_3H_8 versus n-C_5H_{12}/C_3H_8 during flights 6 through 13 of PEM-West A. The lines have the same meaning as in Figure 2a. The intersection of the photochemical and regression lines is arbitrary and placed at the regression fit at the abscissa maximum.

plots but also the rate that hydrocarbon relationships move along the parametric curves. The 2500 pptv background case represents an extreme limit to the relationship, since C_2H_6 does not change with time. For this particular case, the slope of the log-log relationship is identical to that determined by regression in Figure 2a, and the time to reach an arbitrary, low ratio is a minimum. With lower backgrounds the parametric curves start out with steeper slopes, but after about two n-C_4H_{10} lifetimes, the slopes become nearly equivalent to that of the invariant C_2H_6 case. This is of course expected, since C_2H_6 will be close to background and more invariant as time increases, having less of an influence on the ratio relationship. Thus the dilution model implies that the slope of this log-log ratio should approach the value $(K+L_{n\text{-butane}})/(K+L_{propane})$ for those points well removed from the emission source.

According to the simple dilution model expectations of equation (4) the ratio-ratio relationship for the case when all species have negligible backgrounds is independent of the dilution rate (K), and the regression slopes to the log-log plot should yield the ratio of reaction rate differences as originally proposed in the "hydrocarbon clock" approach to HC ratios [*Roberts et al.*, 1984; *Rudolph and Johnen*, 1990; *Parrish et al.*, 1992]. The simple dilution model would explain the departure of the relationships from OH photochemistry shown in Figures 6a and 6b as being a consequence of choosing the wrong hydrocarbons for using correlation statistics to compare with the expectations of OH photochemistry. Figure 7 shows the ratio-ratio relationship for three species (n-C_4H_{10}, n-C_5H_{12}, and C_3H_8) measured during PEM-West A that can safely be assumed to have negligible backgrounds with appropriate filtering. The kinetic slope from OH photochemistry should be 0.52, and the regression slope through the filtered points is 0.66 or only about 25% different and nearly within the 1σ uncertainty of the slope determination. Table 2 summarizes the results of all possible alkane combinations with C_3H_8 used as the denominator. Since there are only five points with n-C_6H_{14} > 30 pptv, the slope estimates using this species are probably not statistically significant. However, there is good agreement (better than 27%) between the OH kinetic slopes and those determined by regression for the remaining combinations. Given the scatter in the data and the probability of nonhomogeneous emission

Table 2. Regression Slopes for Various Combinations of Log(Ratio) Versus Log(Ratio) Correlations

	n-C_4H_{10}(97)	i-C_4H_{10}(67)	n-C_5H_{12}(35)	i-C_5H_{12}(41)	n-C_6H_{14}(5)
n-C_4H_{10}		0.76 ± 0.1	0.66 ± 0.09	0.49 ± 0.12	0.37 ± 0.27
i-C_4H_{10}	0.8 ± 0.1		0.58 ± 0.08	0.57 ± 0.13	0.51 ± 0.13
From OH kinetics	1.	1.	0.52	0.52	0.32

C_3H_8 is the denominator for both abscissa and ordinate. Column 1 gives the ordinate numerator; the top row is the abscissa numerator with number of points > 30 pptv in parentheses.

ratios over the large region of the PEM-West A experiment, this agreement is somewhat surprising and yields two important conclusions. First, OH is undoubtedly the most important species determining the highly reactive alkane relationships. For example, similar to the analysis of *Parrish et al.* [1993], the kinetic slopes [*Atkinson and Aschmann*, 1985] expected for chlorine reactions with the species ratios used in Table 2 have drastically different values than the kinetic slopes for OH reactions. This is particularly true when i-C_4H_{10} is the numerator of the ordinate. In this case, the Cl reaction with i-C_4H_{10} is nearly identical to that of C_3H_8, making the expected slope of the Cl kinetic ratio close to zero. The slopes for the numerator-abscissa combinations of the second row in Table 2 should be less than 0.05 if Cl was the major reactant, but regressions yield values greater than 0.5 as expected from OH kinetics. Considering the expected slopes and uncertainties of the i-C_4H_{10} - pentane combinations in Table 2, a slope < 0.41 would certainly imply a discernable Cl signal in this type of analysis, which would correspond to a Cl/OH ratio of 0.007 to 0.014. An assumed diurnal average [OH] of 2 $\times 10^6$ cm^{-3} yields a detectable [Cl] signal of $<3 \times 10^4$ cm^{-3}, and the results of Table 2 imply a much lower bound to [Cl] for the PEM-West A study. Secondly, there must be something right about the simple dilution model; that is, the assumption that mixing only occurs with background air (containing zero HC in this case) does not seriously compromise its ability to describe the relationships between highly reactive alkanes. This gives additional confidence that the estimate of the dilution rate relative to n-C_4H_{10} oxidation is reasonably accurate and not influenced significantly by hypothetical mixing scenarios that could alter the photochemical relationship.

Section B, Inclusion of Back Trajectories

In this section we include estimated values of the time from emission in order to further examine the PEM-West A hydrocarbon observations and three-dimensional model results within the context of the simple dilution model. Roughly 800 back trajectories and time from the last contact with land or three-dimensional model domain boundary (back to 0000 UT, 9/20/91) are then determined for each time and location of the individual HC canister samples taken from September 22 to October 6, 1991 (flights 6-13).

To adequately test the photochemical-mixing relationship proposed in equation (1), a sufficient sampling of points with clear signals of anthropogenic influence from a relatively isolated region is desirable. Additionally, it is also desirable to have a large range in the time from emission in order to test the simple dilution model over an appropriate dynamic range. For data collected above 2 km, most back trajectories pass over land at altitudes that are not impacted by anthropogenic activity along the coast, so the data used in this analysis are restricted to ~200 samples that were collected below 2 km altitude during flights 6-13. From these data, only 70 of the back trajectories are determined to have land contact times of 4 hours or greater during the September 20 to October 6 period within the model domain. Many of these back trajectories either originated from relatively clean coastal regions or show anthropogenic influence from an isolated source region but exhibit very little variation in the contact time from land. The clearest signals of anthropogenic influence with a wide range of land contact times to a small origination region is from the data collected east of Japan on flights 7 (9/24/91) and 8 (9/25/91). Figure 8 shows the flight tracks of these two flights and the back trajectories for several of the data-collection locations. Eleven of the 70 possible back trajectories originate within a 180-km region close to and north of Tokyo with the height of the origination point determined to be between 1.4 and 2.3 km above sea level. Hydrocarbon values with back trajectories originating 60 km north or south of this region were significantly lower for a given land contact time. The back trajectories also indicate that the winds were fairly steady and persistent during the travel time, so that strong meteorological variations should not be an added complication to consider.

Equations (1) and (2) relating to the simple dilution model imply an exponential decay for the amount of hydrocarbon above a scaled background, or

$$\log_e\left[X-\frac{KX^B}{K+L_X}\right] = \log_e\left[X^0-\frac{KX^B}{K+L_X}\right] - (K+L_X)t \qquad (5)$$

where t is the time from emission. Figures 9a and 9b illustrate the dependence of the observed n-butane, propane, acetylene, and ethane for the 11 points considered in the analysis as a function of contact time from land. While there is some scatter, due mostly to the two low HC sets at 32 and 54 hours from contact, the exponential decay appears to describe the dependence rather well. Moreover, the increasing slope of the decay as hydrocarbon OH reactivity increases is quite obvious. The chemical time constants for ethane and acetylene are long enough that the decrease of these species should be due mostly to mixing, while the more reactive species will have an additional contribution from OH loss. It therefore appears plausible that the observed data can be used to estimate L_X, K, and their relative importance to the exponential decay. However, equation (5) contains the initial concentration upon emission and the background concentration in addition to L_X and K as unknowns.

The term containing the initial concentration represents an offset to the time dependence in equation (5). In a simple regression fit to the points of Figures 9a and 9b, a slope and intercept at t=0 would be determined that best fit the data. However, the initial condition is only with respect to a particular back trajectory's contact with the coastline. Between the time of an air parcel's injection of HC and the time it reaches the coastline, small-scale transport and dilution are expected to significantly influence the HC. Since the intercept or initial condition at t=0 determined from the regression fits are expected to have little connection with the original emissions, they are ignored in this analysis. The dilution and photochemical loss information of immediate interest is contained in the regression slopes, which depend on the undefined background values specified within the formalism. As discussed in the previous section, one can safely assume that for hydrocarbons with sufficiently high OH reactivity the background is negligible. For HC with OH reactivities slower than butane, the PEM-West A data imply there is always a measurable amount originating from ubiquitous hemispheric or continental sources, which may have a measurable impact on the absolute amount observed near more recent emissions. Since equation (5) requires a quantitative assignment to backgrounds for longer-lived HC, how these backgrounds are determined from observations and the sensitivity of the simple dilution model results to the

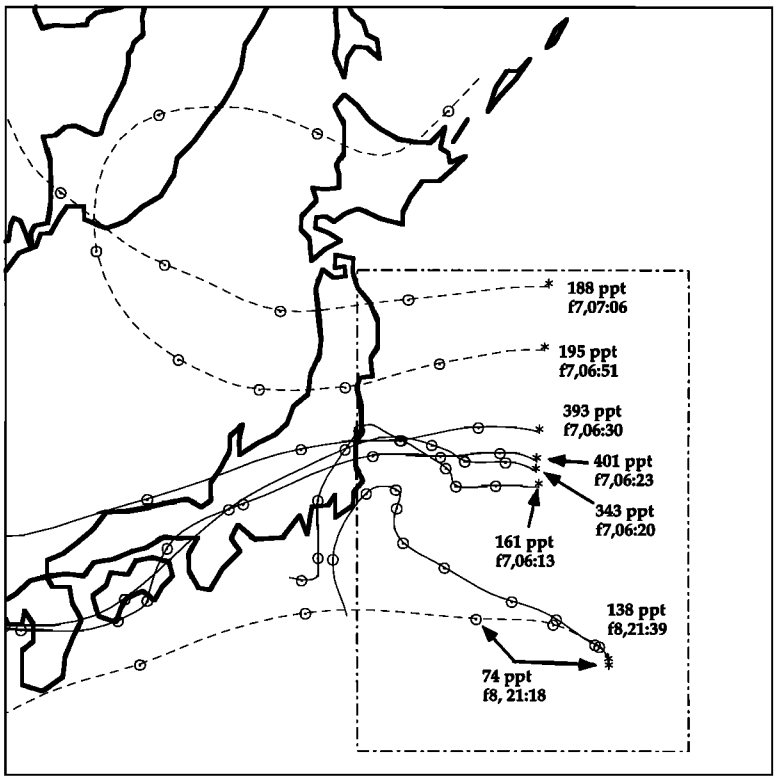

Figure 8. Several back trajectories determined for samples collected off the eastern coast of Japan during flights 7 and 8 of the PEM-West A experiment, all at altitudes less than 1.5 km. Circles along the trajectories are every 12 hours. Next to each destination point is the C_2H_2 mixing ratio, the flight number and universal coordinated time of the samples. Dashed trajectories fall outside the emission region used in the analysis. The dashed box denotes the study area used for the three-dimensional model analysis.

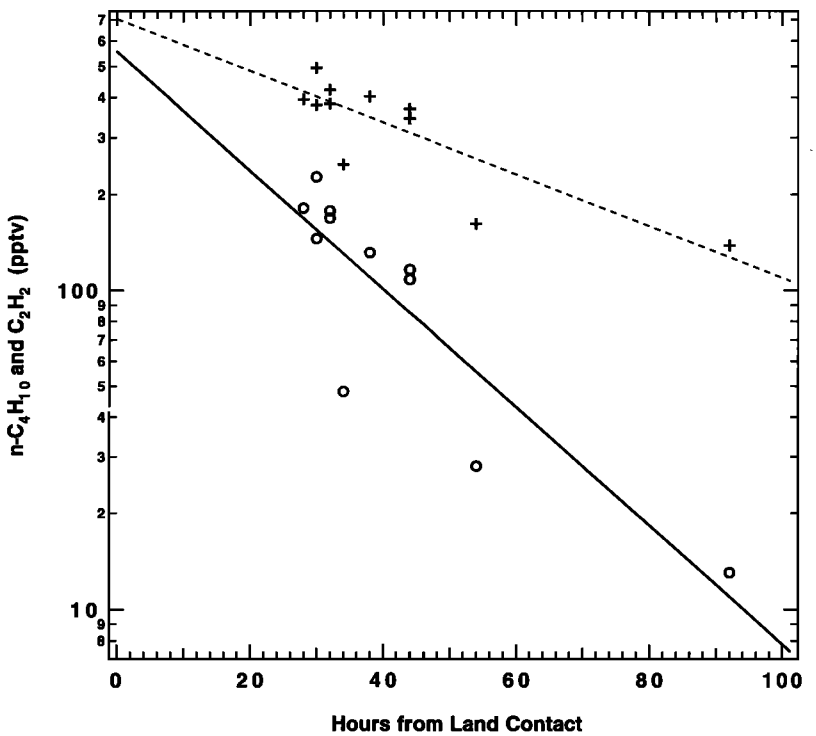

Figure 9a. Mixing ratios of observed n-C_4H_{10} (circles) and C_2H_2 (pluses) for those samples determined to originate from the coastline east and north of Tokyo as a function of time from the coastline as determined from the back trajectories. The lines are best fits to the decay slopes predicted by equation (5) as discussed in the text.

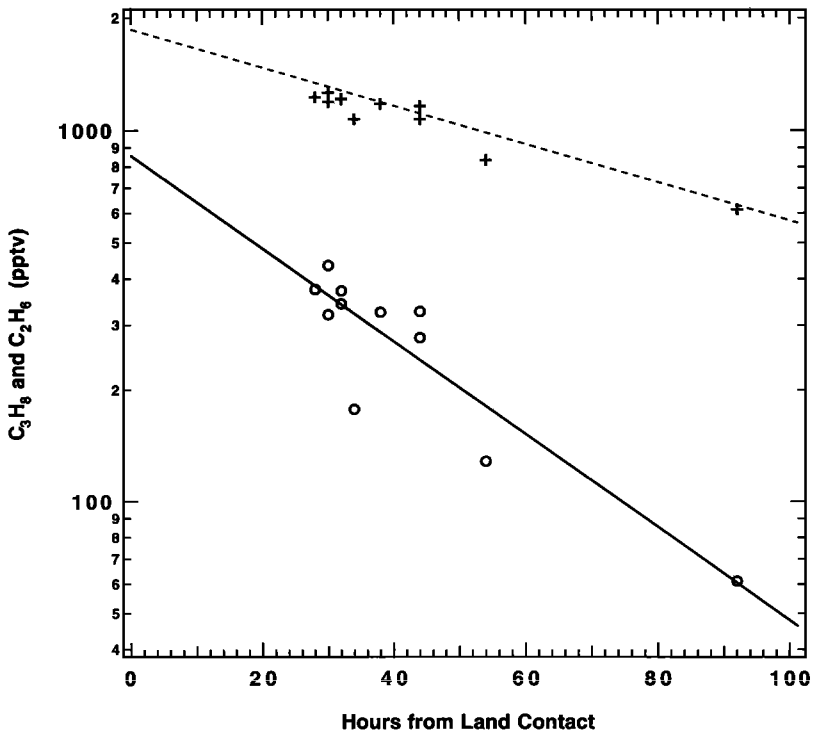

Figure 9b. The same as Figure 9a except for C_3H_8 (circles) and C_2H_6 (pluses).

specified background values therefore becomes an issue. We therefore turn to the three-dimensional model results for guidance in deriving an objective method for background determinations, as a check on the consistency of the simple dilution model, and to examine the sensitivity of results to background assumptions.

Back Trajectories and Hydrocarbons From the Three-Dimensional Model

Model hydrocarbon results are obtained and back trajectories are calculated for the area east of Japan outlined in Figure 8 for 0600 UT, September 4, 1991, roughly the midtime of most of the observations in Figure 9. Analogous to the filters applied to the observed data, only data below 2 km and with back trajectories originating from the same 180 km of coastline are used in the three-dimensional model analysis. Figures 10a and 10b show the decay plots for the same hydrocarbons shown in Figure 9. The stronger decay slopes for more reactive hydrocarbons are evident in the figures.

As discussed in the previous section, the simple dilution model is able to reproduce relationships between nonreactive species quite accurately due to the linear nature of the dilution process in the absence of photochemical loss. Thus the background concentrations are well defined by the boundary conditions, there is an unambiguous determination of the terms on the left hand side of equation (5) from the three-dimensional model results, and the slope of a linear least squares fit to the logarithm of the amount of inert material above background versus contact time determines the dilution coefficient. Applying this procedure to the inert analogs of the species listed in Table 1 results in a derived K of 0.016 ± .004 $hour^{-1}$ for the three-dimensional model, or a characteristic lifetime for dilution of 2.6 ±0.6 days, independent of the species used in the least squares fit. Although this quantity is a characteristic of the numerical model's net transport for only a particular location and 2-day period, it is interesting to compare this characteristic time with the photochemical lifetimes in Table 1. The timescale for the dilution process is faster than that of photochemistry for all species with OH reactivity less than n-butane, which explains why photochemistry appears to have only a secondary effect in determining the three-dimensional model HC relationships in Figures 3b and 5b.

Once K is known, the three-dimensional model average [OH] can be determined unambiguously from linear least square fits of n-butane and toluene decay, since the background mixing ratios of these two species are set to be near zero. Subtracting K from the best fit slopes and dividing by OH reactivity yields an [OH] of 2.5 (±0.9) $\times 10^6$ and 2.1 (±0.5) $\times 10^6$ cm^{-3} from n-butane and toluene, respectively. The [OH] derived by averaging OH values calculated from the three-dimensional photochemical model from 0 to 2 km over the September 23-24 2-day cycle within the outlined study area of Figure 8 is 2.1 $\times 10^6$ cm^{-3}. The [OH] derived from the hydrocarbon slopes is therefore exactly what is expected from a strict Eulerian perspective within the uncertainties of the determination.

With K and [OH] known, background values of C_3H_8, C_2H_2,C_2H_6, and CO can be estimated that give the closest determination of the [OH] value independently derived by temporal and spatial averaging. A subset of model data points that represent air masses with a minimum of anthropogenic influence are first selected, from which background values should be chosen. These points are located between 0 and 2 km and are determined by back trajectories to have had no land contact for at least 96 hours (~ 900 points within the study area outlined in Figure 8). Figures 11a and 11b show the location

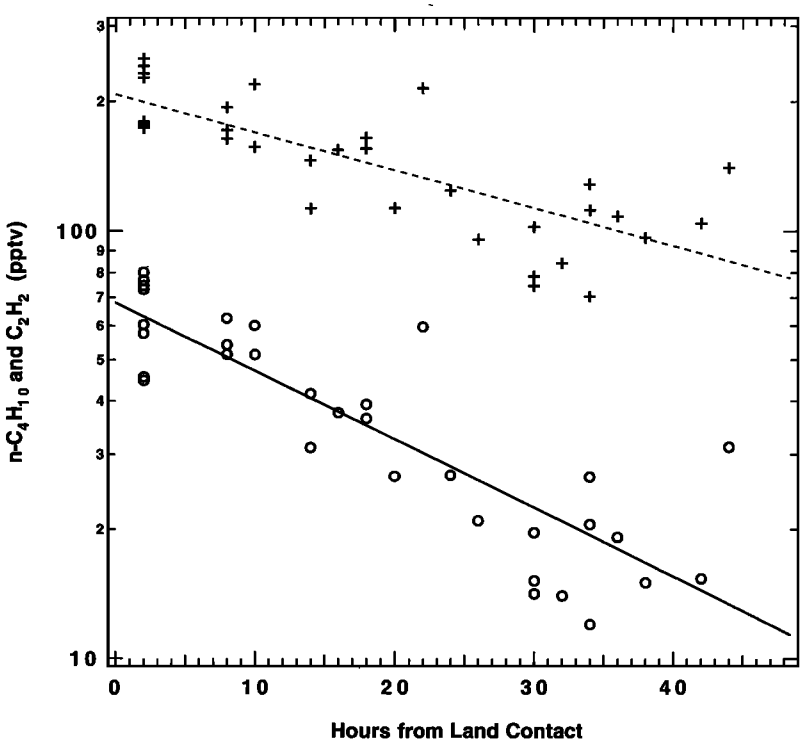

Figure 10a. Mixing ratios of n-C_4H_{10} (circles) and C_2H_2 (pluses) determined from the three-dimensional model for those points determined to originate from the coastline east and north of Tokyo as a function of time from the coastline as determined from the back trajectories.

of the median, lower quartile, and minimum for C_2H_6 and C_2H_2 within this ensemble of points. These figures also show the dependence of the least square determinations of [OH] on the background value assigned to either C_2H_6 or C_2H_2, assuming K=0.0161 $hour^{-1}$. The uncertainty limits in the figures are derived from the propagation of the 1σ uncertainty from the regression slope determination and the 25% 1σ uncertainty in the determination of K outlined above. The uncertainty in the slope determinations results in quite large uncertainties in OH for both species but more so for C_2H_6,

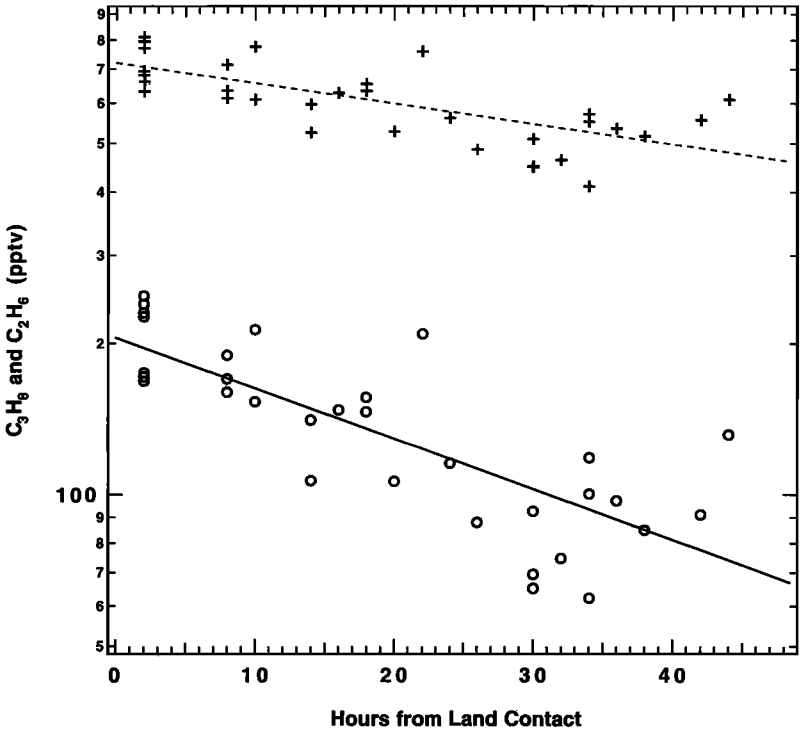

Figure 10b. The same as Figure 10a except for C_3H_8 (circles) and C_2H_6 (pluses).

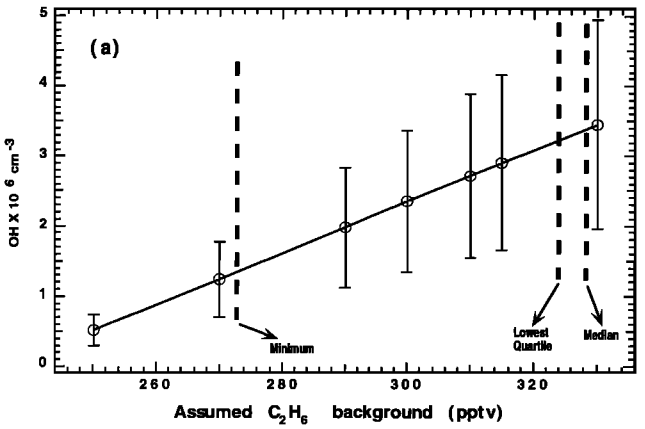

Figure 11a. The sensitivity of OH determined from regression analysis of n-C_4H_{10} and C_2H_6 from the three-dimensional model results as a function of the assumed background of C_2H_6. The dilution coefficient has been fixed to 0.016 hour^{-1}. The dashed lines give the locations along the abscissa of the minimum, lower quartile, and median within the cummulative distribution of samples having oceanic back trajectories > 4 days, as discussed in the text.

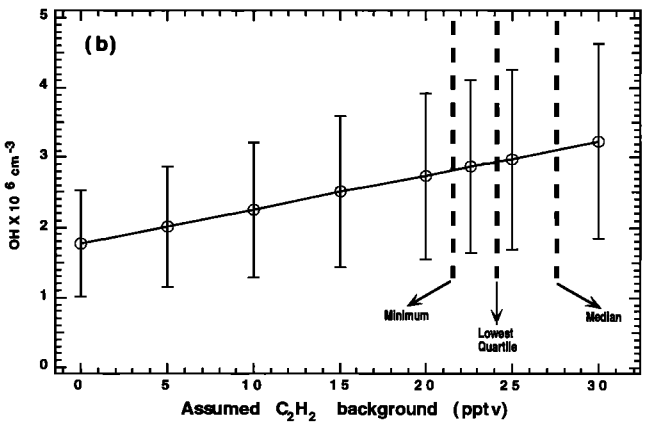

Figure 11b. Same as Figure 11a except OH is determined from the regression analysis of n-C_4H_{10} and C_2H_2.

since the 25-day photochemical lifetime of C_2H_6 makes it difficult to extract the small OH decay signal relative to the dilution term. The uncertainty for both species is large enough to say that any value between the median and the minimum of the clean-maritime air points would be appropriate as a background, but a background close to the ensemble minimum would retrieve the desired [OH] value of 2.3 $\times 10^6$ cm^{-3}. The [OH] determined from C_2H_6 is very sensitive to small changes in the assumed background, while acetylene is much less so. Similar results apply to C_3H_8 (low sensitivity below the clean-air median of 14 pptv, 70% [OH] uncertainty) and CO (high sensitivity and high uncertainty) both estimating [OH] better at the lowest possible background values. The high sensitivity to CO and C_2H_6 is actually a consequence of the mixing ratios being close to the assumed background. The lowest values of C_2H_6 and C_2H_2 to originate from Japan in Figure 11 are 410 and 70 pptv, respectively, while the median of the clean-oceanic background values are 329 and 27 pptv. Thus a 20% change in the ethane background will have a larger impact on the amount of C_2H_6 above background than for C_2H_2. A useful measure of the relative uncertainty due to the background assumption may therefore be expressed as

$$\text{relative backg. uncertainty} = \frac{\text{median}_{\text{clean}} - \text{minimum}_{\text{clean}}}{\text{minimum}_{\text{plume}} - \text{median}_{\text{clean}}}$$

where the median or minimum is with respect to the set of points determined from back trajectories to originate from either clean-oceanic sources or the anthropogenic plume. This relative uncertainty is 0 for n-C_4H_{10} and toluene and 0.12, 0.14, 0.68 and 48. for C_3H_8, C_2H_2, C_2H_6, and CO, respectively. Thus there is a clear distinction between the more reactive C_3H_8 and C_2H_2, which are decidedly above the median of the clean-air values, and the less reactive C_2H_6 and CO that are only marginally above a possible background.

Back Trajectories and Hydrocarbons From Observations

With these three-dimensional model results as a guide, the simple dilution model can be applied to the observations. First, the background of a given hydrocarbon is defined, based on back-trajectories below 2 km that have not had land contact for at least 96 hours from all the observations between 9/22/91 and 10/6/91 (~26 samples). The average over the lowest quartile of these clean, marine-air values is chosen to represent the background concentration in keeping with the three-dimensional model results. These statistically determined backgrounds and the associated relative background uncertainty for the Tokyo plume are given in the last two columns of Table 3a. For hydrocarbons with OH reactivities

Table 3a. [OH] $\times 10^6$ cm^{-3} Determined From Pairs of Hydrocarbons

	toluene	n-C_6H_{14}	n-C_5H_{12}	i-C_5H_{12}	n-C_4H_{10}	i-C_4H_{10}	C_6H_6	C_3H_8	C_2H_2	back-ground	relative uncertainty
n-C_4H_{10}	X	3.3±2.0	X	2.7±3.6						0.	0.
i-C_4H_{10}	X	3.3±2.0	X	2.8±3.5						0.	0.
C_6H_6	0.31±1.1	3.7±1.4	X	3.6±1.8	X	X				9.7 ppt	.28
C_3H_8	X	3.0±1.2	5.0±2.5	2.5±1.4	2.3±2.3	2.2±2.2	X			10.1 ppt	.13
C_2H_2	0.5±0.9	3.4±1.1	5.4±2.2	3.2±1.3	3.6±1.9	3.5±1.8	1.4±6.2	X		28.4 ppt	.14
CO	0.33±1.	3.1±1.2	4.8±2.2	2.8±1.4	2.8±2.0	2.7±1.9	.6±4.2	4.0±4.4	X	69.5 ppb	.04
C_2H_6	0.5±0.7	3.2±.8	4.9±1.7	2.9±.9	3.0±1.1	3.0±1.1	1.3±2.4	4.5±2.1	1.0±3.1	352. ppt	.15
C_2Cl_4	0.6±1.	3.2±1.2	4.9±2.1	3.0±1.4	3.2±1.9	3.1±1.8	1.8±3.9	4.5±4.0	2.2±5.9	2.3 ppt	.23
CH_3CCl_3	0.9±1.	3.4±1.1	5.0±2.1	3.3±1.3	3.6±1.8	3.5±1.7	2.7±3.4	5.2±3.5	3.6±4.8	142. ppt	.42
CH_4	0.6±0.8	3.2±.9	4.7±1.8	2.9±1.	3.0±1.4	2.9±1.3	1.5±2.6	4.0±2.4	1.6±3.3	1709. ppb	.05

X denotes nonconvergence of the algorithm that determines [OH] and K for each pair. Backgrounds and relative background uncertainties are given in columns 11 and 12. See text for details.

Table 3b. K^{-1}, the Characteristic Time for Dilution (Days) Determined From Pairs of Hydrocarbons

	toluene	n-C_6H_{14}	n-C_5H_{12}	i-C_5H_{12}	n-C_4H_{10}	i-C_4H_{10}	C_6H_6	C_3H_8	C_2H_2
n-C_4H_{10}	X	3.1±6.1	X	2.3±5.2					
i-C_4H_{10}	X	3.3±6.5	X	2.5±5.6					
C_6H_6	1.8±1.	7.9±19.	X	7.8±20.	X	X			
C_3H_8	X	2.1±1.	3.6±4.4	2.0±0.9	1.9±1.1	1.8±1.1	X		
C_2H_2	2.1±0.7	3.7±2.4	8.4±17.	3.5±2.3	3.9±3.5	3.8±3.2	2.4±3.1	X	
CO	1.9±0.9	2.4±1.4	3.0±2.1	2.4±1.3	2.4±1.4	2.4±1.4	1.9±1.2	2.7±2.1	X
C_2H_6	2.2±0.3	2.8±0.4	3.3±0.8	2.7±0.4	2.7±0.5	2.7±0.4	2.3±0.5	3.2±0.8	2.3±0.6
C_2Cl_4	2.6±1.4	3.0±1.9	3.2±2.3	2.9±1.8	3.0±1.9	3.0±1.9	2.8±1.9	3.2±2.5	2.8±2.2
CH_3CCl_3	3.9±3.1	4.0±3.2	4.1±3.3	4.0±3.2	4.0±3.2	4.0±3.2	4.0±3.2	4.1±3.3	4.0±3.2
CH_4	2.4±0.7	2.7±0.8	2.9±0.8	2.6±0.8	2.6±0.8	2.6±0.8	2.5±0.7	2.8±0.8	2.5±0.7

X denotes nonconvergence of the algorithm that determines [OH] and K for each pair. See text for details.

equal to or larger than n-C_4H_{10}, the background is assumed to be zero. Because there is still uncertainty and high dependence of results on the chosen background for the slowly reacting HC, it is instructive to present the results by examining [OH] and K determined from individual hydrocarbon pairs and to look for consistency or patterns for results derived from one hydrocarbon against all others.

The determination of [OH] and K according to the simple dilution model for two sets of HC observations is fairly straightforward. When the backgrounds of two HC are defined, equation (5) for hydrocarbon X and a second similar equation for hydrocarbon Y contain the unknowns K and [OH], since L_X and L_Y are related by their OH reactivities. Thus for every pair of HC there are two equations and two unknowns, K and [OH]. However, an iterative procedure must be used to solve the pair of equations, since the unknowns are both within and outside the logarithm terms in equation (5). Within the iterative procedure, a guess is first made for [OH] and K, thus defining the scaled concentration terms on the left-hand side of equation (5). A linear least squares of the logarithmic decay of these scaled concentrations versus land contact time is then performed on each HC, yielding new estimates of $(K + L_x)$ and $(K + L_y)$, from which updated K and [OH] are determined. The process is repeated until a convergence criteria (0.5%) is reached in [OH]. This iterative procedure converges so long as there is reasonable separation in the reactivities of the two hydrocarbons and there is not excessive scatter in the hydrocarbon decay slopes. The iterative procedure is also independent of the initial guesses to [OH] and K, provided they fall within realistic limits of zero and the maximum possible value deduced from the decay slope of either species. As mentioned previously, the intercept value is allowed to be determined in the regression fit but is ignored in this analysis. The lines in Figures 9 and 10 are examples of the best-fit determinations by the iterative procedure for those particular HC pairs.

Tables 3a and 3b present the results of [OH] and K derived from separate hydrocarbon pairs, along with the background used in the calculations. Uncertainties for both K and [OH] represent 1σ uncertainties derived from the propagation of 1σ uncertainties of the slope determinations from the regression fit of the last iteration. It should be emphasized that there are additional uncertainties in the HC background values, rate constants, the measurements themselves, the land contact time, and trajectory origin that are not included in these uncertainty estimates. As discussed with regard to the three-dimensional model results, uncertainty due to the background assumption can be significant but is easily comparable between the various HC by the relative background uncertainty defined previously. From the three-dimensional model results, a species with a relative background uncertainty less than 0.15 will have a smaller uncertainty associated with the background than with the statistical scatter of the data. Measurement uncertainties of species having concentrations close to the detection limit (e.g., toluene, n-C_6H_{14}, and pentanes) should be reflected somewhat in the statistical scatter of the data. Compared to the relatively large uncertainty generated by the statistical scatter attributable to the small sampling size (11 points), the other sources of uncertainty are expected to be minor. Nonetheless, the uncertainties quoted in Tables 3a and 3b are due only to the statistical scatter of the data and should be considered lower limits.

There are several features within Tables 3a and 3b that deserve comment. First, either the slope-fitting algorithm does not converge or there is greater than 100% uncertainty when the OH reactivities of the individual pairs are close to each other. Determinations based on C_3H_8 as the most reactive species are only marginally useful, and determinations based on species with any lower OH reactivity (e.g., C_2H_2) possess too high an uncertainty. Secondly, there are obvious trends in the determination for specific hydrocarbons used in the analysis. All of the [OH] values based on toluene are systematically lower than from other hydrocarbons. In fact, the decay slope of toluene is less than that of n-hexane or the pentanes, which does not seem possible since its OH reactivity is the fastest of these species. Assuming the kinetic data for toluene is not off by more than 50% and there is no selective input of toluene along the trajectory, the only possible explanation is a systematic bias in the toluene measurements, which is close to the detection limit for many of the samples used in this analysis. Similarly, [OH] values based on n-pentane are systematically higher than for other HC; however, the large uncertainty and the fact that samples were close to the detection limit precludes a definitive difference to be ascribed to n-pentane in relation to the other HC. All of the characteristic dilution time determinations based on CH_3CCl_3 as the least reactive HC are systematically higher than with other HC. In this case, the relative uncertainty in the background is higher than all other HC. An 8% increase in the adopted background would reduce the characteristic dilution times by 25% and feed back into the [OH] determinations based on this species. In contrast to the three-dimensional

model results the observations of CO, CH_4, and C_2H_6 have small relative background uncertainties and should be the most reliable species to use as the least reactive HC.

In deriving a best estimate of [OH] and the characteristic dilution time, estimates within Table 3 having greater than 100% uncertainty in either [OH] or K are discarded. Because of the high sensitivity of CH_3CCl_3 to the assumed background, estimates involving this species are also discarded. The resulting uncertainty-weighted estimate of [OH] from all remaining HC pairs is $3.2\pm1.4 \times10^6$ cm^{-3}, and the uncertainty-weighted characteristic dilution time is 2.8±0.4 days. Thus as is the case for the three-dimensional results, fitting the observations to the simple dilution model implies a very strong contribution of the dilution term, particularly for those species with OH reactivities less than n-butane. In comparison to the three-dimensional model results, the [OH] from the observations is ~50% higher, which could easily be explained by the coarse treatment of NMHC emissions within the model, particularly the naturally occurring NMHC, or other factors such as the prediction of cloudiness within the mesoscale model and the treatment of the cloud's effect on photolysis rates. On the other hand, the characteristic times for dilution are quite similar between the three-dimensional results and the observations. Within the three-dimensional model, vertical redistribution due to mixing within the PBL is the largest term contributing to dilution in the lowest 1-2 km. Above the PBL, numerical diffusion within the advection scheme usually dominates the horizontal eddy diffusion term near large mixing ratio gradients. Therefore the agreement between the three-dimensional model and the observations for the dilution term may be fortuitous.

Summary and Conclusions

A unique aspect of the PEM-West A experiment is the anthropogenic signal often detected in air masses over the western Pacific Ocean, well removed from emission sources. Measurements of hydrocarbons, particularly in the lower troposphere where source regions are clearly identifiable, are quite useful due to their association with anthropogenic activity and well-understood photochemistry. Other papers within this issue have utilized hydrocarbon relationships as markers in the photochemical interpretation of various air masses, and also as a basis for air mass classification schemes. This paper uses the hydrocarbon observations to understand and derive more fundamental quantities, in particular the rate of atmospheric dilution and OH concentrations controlling the photochemical loss. With the aid of three-dimensional photochemical model results this paper also outlines which hydrocarbons, hydrocarbon relationships, and practical methodologies are useful for estimating these fundamental quantities.

If all of the dynamic and meteorological phenomena leading to atmospheric mixing are compressed into a single quantity (a dilution coefficient), then a simple conceptual model can be formulated that relates the evolution of hydrocarbon concentrations to photochemical loss and this dilution term. The three-dimensional model results and observations have been used to illustrate the applicability of this simple dilution model. The biggest drawback is related to the definition of a background air mass and the concentration of individual hydrocarbons therein. If the hydrocarbons being considered have reasonably high OH reactivity and one can safely assume background concentrations are insignificant, the dilution model is expected to be more applicable to the real atmosphere. The PEM-West A measurements of the highly reactive alkanes (C_3 to C_6) are therefore used as the observational basis for deriving the relative dilution rate and testing the applicability of the simple dilution model for the lower tropospheric data set in the vicinity of eastern Asia. To eliminate any possible bias from measurement imprecision or inaccuracy, only data significantly greater than the detection limits are included in the analysis. In terms of the highly reactive hydrocarbons, several features of the three-dimensional model results and observations are similar and consistent with the simple dilution model.

According to the dilution model for species with insignificant backgrounds, regression fits to the log of one species versus another or the log of a ratio versus the log of a species yields a quantitative determination of the dilution coefficient, relative to the loss rate of a particular hydrocarbon. Comparing one species versus another, both the three-dimensional model results and the observations are consistent with an average rate of dilution roughly equivalent to n-butane oxidation for the western Pacific lower troposphere during solstice. This result is also consistent among the various possible combinations of highly reactive alkane pairs afforded by the hydrocarbon observations. Since dilution apparently has such a large effect, this result has negative implications for the use of hydrocarbon ratios as photochemical clocks, particularly with hydrocarbons having OH reactivity less than butane. Similarly, hydrocarbon ratios used as markers of atmospheric processing such as C_2H_2/CO or C_3H_8/C_2H_6 should be considered largely a measure of atmospheric dilution with photochemistry playing only a minor part. The role of dilution in affecting other photochemical relationships, i.e., between NO_y, NO_x, CO, and O_3, is an obvious direction for future study.

For negligible backgrounds the dilution model predicts that the regression slope determined from the logarithm of one ratio versus that of another depends only on the photochemical loss rates and not on the history of dilution and mixing that occurs downwind of the source. The observed data fit the expectation of dominant OH kinetics affecting the hydrocarbon ratio relationship, and this result is consistent between various combinations of reactive alkanes used in the ratios. Equivalent regressions to the three-dimensional model results also yield the OH photochemical rate relationship imposed by the model formulation. This is a clear indication that the observations do conform to the expectations of the dilution model, but comparing one ratio to another yields no information on the relative importance of photochemistry and dilution.

No attempt has been made in this study to fit a large set of the less reactive hydrocarbons to the dilution model as was done for the more reactive alkanes. This is because a background value must be assigned for each hydrocarbon, and the simple dilution model cannot be expected to adequately treat the statistical nature of real-world atmospheric mixing processes. Although this is also true of for the highly reactive hydrocarbons, the atmosphere is always mixing emissions toward the zero background for these HC, except in the transient event of plume overlap. In the case of less reactive species the background concentration is probably a complicated function of latitude, longitude, and season.

Given this conceptual difficulty and the fact that any regression analysis depends strongly on the chosen background, only qualitative comparisons between three-dimensional results and various HC relationships from the measurements of less reactive HC are examined. However, one valuable interpretation of ratio versus ratio relationships previously studied should be mentioned. For the case of $n\text{-}C_4H_{10}/C_2H_6$ versus C_3H_8/C_2H_6 the dilution model predicts that the regression slope should lie between the photochemical and the inert-dilution limits simply because of the high background for C_2H_6. If an appropriate background were subtracted from C_2H_6 in the ratios, then the expected photochemical decay slope could theoretically be determined by the modified regression slope.

The inclusion of back-trajectory analysis for both the three-dimensional results and the observations allows for the absolute determination of rates by introducing time into the analysis of hydrocarbon decay measurements. Within the entire PEM-West A hydrocarbon data set, only a very limited number of points (eleven) were determined to have arrived from a contiguous source region with sufficient anthropogenic signal and a sufficient range of land contact times to allow meaningful statistics. These points originated from the Tokyo region and determined to be sampled from 2 to 4 days after last contact with the coastline. Clearly, a measurement platform and experiment specifically designed to study the evolution of pollution plumes into an ocean basin would be desirable to obtain better statistics and further test the analysis procedure presented here. Designed more as a survey experiment, it is only by happenstance that the PEM-West A mission was able to encounter and collect the available samples from the Tokyo plume used in this analysis. The decrease of inert species from the three-dimensional model for a sample of points originating from the same location results in the determination of a dilution coefficient that has a characteristic time of ~2.5 days, independent of the inert species chosen in the regression. With this dilution rate the three-dimensional model decreases of n-butane and toluene are both consistent, to within 20%, of the 2.1×10^6 cm^{-3} average OH determined from averaging the model OH field directly. Applying the dilution rate and OH concentration to the other three-dimensional model species that have a significant background shows that the best choice of a background value to use in regression fits corresponds to the lowest values of that hydrocarbon in the model domain. With these three-dimensional model results as a guide, a methodology is developed to derive the dilution coefficient and OH concentration from the 11 samples based on fitting the decay rates of observed hydrocarbon pairs. The results are reasonably consistent between various hydrocarbons, and yield an average OH of 3.2×10^6 cm^{-3} for the 3-day period September 23-25, 1991, in the lowest 2 km, for the study area east of Japan shown in Figure 8. The characteristic time for dilution is determined to be ~2.8 days, which is quite consistent with the three-dimensional model results from the same area. Assuming the average OH for the western Pacific is 1.5 to 2×10^6 cm^{-3}, the dilution coefficient determined from the regression of all the hydrocarbon observations below 4 km is also quite consistent with this estimate.

Acknowledgements. This research was supported in part by the Atmospheric Chemistry Project of the Climate and Global Change Program of the National Oceanic and Atmospheric Administration and by the NASA Global Tropospheric Experiment. We thank Michael Trainer, David Parrish, and B. T. Jobson for useful discussions. We also greatly appreciate the thoughtful considerations and comments of both reviewers.

References

Anthes, R. A., E.Y. Hsie, and Y-H Kuo, Description of the Penn State/NCAR mesoscale model version 4 (MM4), *NCAR Tech. Note, NCAR/TN-282+STR*, 66 pp., Natl. Cent. for Atmos. Res., Boulder, Colo., 1987.

Atkinson, R., and S. M. Aschmann, Kinetics of the gas phase reaction of Cl atoms with a series of organics at 296±2 K and atmospheric pressure, *Int. J. Chem. Kinet., 17*, 33-41, 1985.

Atkinson, R., Gas-phase tropospheric chemistry of organic compounds: A review, *Atmos. Environ., 24(A)*, 1-41, 1990.

Bamber, D. J., P. G. W. Healey, B. M. R. Jones, S. A. Penkett, A. F. Tuck and G. Vaughan, Vertical profiles of tropospheric gases: Chemical consequences of stratospheric intrusions, *Atmos Environ., 18*, 1756-1799, 1984.

Blake, D. R., and F. S. Rowland, Global atmospheric concentrations and source strengths of ethane, *Nature, 321*, 231-233, 1986.

Blake, N., S. A. Penkett, K.C. Clemitshaw, P. Anwyl, P. Lightman, and A.R.W. Marsh, Estimates of atmospheric hydroxyl radical concentrations from the observed decay of many reactive hydrocarbons in well-defined urban plumes, *J. Geophys. Res., 98*, 2851-2864, 1993.

Blake, D. R., T.W. Smith, Jr., C.J.-L. Wang, O.W. Wingenter, N.J. Blake, F.S. Rowland, and E.W. Mayer, Three-dimensional distributions of nonmethane hydrocarbons and halocarbons over the northwestern Pacific during the 1991 PEM-West A, *J. Geophys. Res.*, this issue.

Brost, R. A., The sensitivity to input parameters of atmospheric concentrations simulated by a regional chemical model, *J. Geophys. Res., 93*, 2371-2387, 1988.

Browell, E. V., et al., Large-scale air mass characteristics observed over the western Pacific during summertime, *J. Geophys. Res.*, this issue.

Calvert, J.G., Hydrocarbon involvement in photochemical smog formation in Los Angeles atmosphere, *Environ. Sci. Technol., 10*, 256-262, 1976.

Crawford, J., et al., Photostationary state analysis of the NO_2-NO system based on airborne observations from the western and central North Pacific, *J. Geophys. Res.*, this issue.

DeMore, W.B., M.J. Molina, S.P. Sander, D.M. Golden, R.F. Hampson, M.J. Kurylo, C.J. Howard, and A.R. Ravishankara, Chemical kinetics and photochemical data for use in stratospheric modeling, in *Evaluation 10, JPL Publ. 92-20*, Jet Propul. Lab., Pasadena, Calif., 1992.

Dignon, J., NO_x and SO_x emissions from fossil fuels: A global distribution, *Atmos. Environ., (26A)*, 1157-1164, 1992.

Environmental Protection Agency (EPA), The 1985 NAPAP emissions inventory (version 2): Development of the annual data and modelers' tapes, Tech *Rep. EPA-600/7-89-012a*, 692 pp., Natl. Tech. Info. Serv., Springfield, Va., 1989.

Gregory, G. L., A.S. Bachmeier, D.R. Blake, B.G. Jeikes, D.C. Thornton, J.D. Bradshaw, and Y. Kondo, Chemical signatures of aged Pacific marine air: Mixed layer and free troposphere as measured during PEM WestA, *J. Geophys. Res.*, this issue.

Hoell, J. M. Jr., et al., Pacific Exploratory Mission-West (PEM-West A): September-October 1991, *J. Geophys. Res.*, this issue.

Jobson, B. T., Z. Wu, L. A. Barrie, and H. Niki, Seasonal trends of isoprene, C_2-C_5 alkanes, and acetylene at a remote boreal site in Canada, *J. Geophys. Res., 99*, 1589-1599, 1994.

Kato, N., and H. Akimoto, Anthropogenic emission of SO_2 and NO_x in Asia: Emission inventories, *Atmos. Environ., 26(A)*, 2997-3017, 1992.

Levy, H., Normal atmosphere: Large radical and formaldehyde concentrations predicted, *Science, 173*, 141, 1971.

Lin, X., B. A. Ridley, J. Walega, G. F. Hübler, S. A. McKeen, E. Y. Hsie, M. Trainer, F. C. Fehsenfeld, and S. C. Liu, A parameterization of subgrid scale convective cloud transport in a mesoscale regional chemistry model, *J. Geophys. Res., 99*, 25,615-25,630, 1994.

Liu, S. C., et al.,Model study of tropospheric trace species distributions during PEM-West A, *J. Geophys. Res.*, this issue.

Logan, J. A., M. J. Prather, S. C. Wofsy, and M. B. McElroy, Tropospheric chemistry: A global perspective, *J. Geophys. Res.*, *86*, 7210-7254, 1981.

Lovelock, J. E., Ionisation methods for the analysis of gases and vapors, *Analt. Chem.*, *33*, 162-178, 1961.

Lurmann, F. W., A. C. Lloyd, and R. Atkinson, A chemical mechanism for use in long-range transport/acid deposition computer modeling, *J. Geophys. Res.*, *91*, 10,905-10,936, 1986.

McKeen, S.A., and S. C. Liu, Hydrocarbon ratios and photochemical history of air masses, *Geophys. Res. Lett.*, *20*, 2363-2366, 1993.

McKeen, S.A., Trainer, M, E.Y. Hsie, R.K. Tallamraju, and S.C. Liu, On the indirect determination of atmospheric OH radical concentrations from reactive hydrocarbon measurements, *J. Geophys. Res.*, *95*, 7493-7500, 1990.

McKeen, S.A., E.-Y. Hsie, M. Trainer, R. Tallamraju, and S.C. Liu, A regional model study of the ozone budget in the eastern United States, *J. Geophys. Res.*, *96*, 10,809-10,845, 1991.

McKenna, D.S., C. J. Hord, and J. M. Kent, Hydroxyl radical concentrations and Kuwait oil fire emission rates for March 1991, *J. Geophys. Res.*, in press, 1995.

Merrill, J. T., Trajectory results and interpretation for PEM-West (A), *J. Geophys. Res.*, this issue.

Nelson, P.F., and S.M. Quigley, Non-methane hydrocarbons in the atmosphere of Sydney, Australia, *Environ. Sci. Technol.*, *16*, 650-655, 1982.

Parrish, D.D., C.J. Hahn, E.J. Williams, R.B. Norton, F.C. Fehsenfeld, H.B. Singh, J.D. Shetter, B.W. Gandrud, and B.A. Ridley, Indications of photochemical histories of pacific air masses from measurements of atmospheric trace species at Point Arena, California, *J. Geophys. Res.*, *97*, 15,883-15,902, 1992.

Parrish, D.D., C.J. Hahn, E.J. Williams, R.B. Norton, F.C. Fehsenfeld, H.B. Singh, J.D. Shetter, B.W. Gandrud, and B.A. Ridley, Reply, *J. Geophys. Res.*, *98*, 14,995 - 14,997, 1993.

Roberts, J.M., F.C. Fehsenfeld, S.C. Liu, M.J. Bollinger, C. Hahn, D.L. Albritton, and R.E. Sievers, Measurements of aromatic hydrocarbon ratios and NO_x concentrations in the rural troposphere: Observations of air mass photochemical aging and NO_x removal, *Atmos. Environ.*, *18*, 2421-2432, 1984.

Roberts, J.M., R.S. Hutte, F.C. Fehsenfeld, D.L. Albritton, and R.E. Sievers, Measurements of anthropogenic hydrocarbon concentration ratios in the rural troposphere: Discrimination between background and urban sources, *Atmos. Environ.*, *19*, 1945-1950, 1985.

Rudolph, J., and F.J. Johnen, Measurements of light atmospheric hydrocarbons over the Atlantic in regions of low biological activity, *J. Geophys. Res.*, *95*, 20,583-20,591, 1990.

Singh, H.B., J.R. Martinez, D.G. Hendry, R.J. Jaffe, and W.B. Johnson, Assessment of the oxidant-forming potential of light saturated hydrocarbons in the atmosphere, *Environ. Sci. Technol.*, *15*, 113-119, 1981.

Smolarkiewicz, P.K., A fully multidimensional positive advection transport algorithm with small implicit diffusion, *J. Comput. Phys.*, *54*, 325-362, 1984.

Smyth, S., et al., Comparison of free tropospheric western Pacific air mass classification schemes for the PEM-West A experiment, *J. Geophys. Res.*, this issue.

State Statistical Bureau of China (SSBC), *The Yearbook of Energy Statistics of China 1989* (in Chinese), China Stat. Publ., Beijing, 1990.

Talbot, R. W., et al., Chemical characteristics of continental outflow from Asia to the troposphere over the western Pacific Ocean during September-October 1991: Results from PEM-West A, *J. Geophys. Res.*, this issue.

Trainer, M., et al., Correlation of ozone with NOy in photochemically aged air, *J. Geophys Res*, 98, 2917-2925, 1993.

United Nations (UN), *World Energy Statistics and Balances 1985-1988*, 386 pp., Int. Energy Agency/Org. Econ. Coop. Dev. (IEA/OECD), Paris, 1990.

D. R. Blake, Department of Chemistry, University of California, Irvine, CA 92717.

J. D. Bradshaw and S. Smyth, Georgia Institute of Technology, Atlanta, GA 30332.

G. L. Gregory, Atmospheric Sciences Division, NASA Langley Research Center, Hampton, VA 23665

E.-Y. Hsie, X. Lin, S. C. Liu and S. A. McKeen (corresponding author), Aeronomy Laboratory, National Oceanic and Atmospheric Administration, R/E/AL4, 325 Broadway, Boulder, CO 80303-3328

(Received December 12, 1994; revised August 31, 1995; accepted September 1, 1995.)